Dynamic stiffness method and CUF-based component-wise theories applied to free vibration analysis of solid beams, thin-walled structures and reinforced panels

(Article begins on next page)

20 September 2024

Dynamic stiffness method and CUF-based component-wise theories applied to free vibration analysis of solid beams, thin-walled structures and reinforced panels

Xiao Liu[a,b,c,d], Alfonso Pagani[d], Erasmo Carrera[d], Xiang Liu[a,b,c,*]

[a]*Key Laboratory of Traffic Safety on Track, Ministry of Education, School of Traffic & Transportation Engineering, Central South University, Changsha, China*
[b]*Joint International Research Laboratory of Key Technology for Rail Traffic Safety, Central South University, Changsha, China*
[c]*National & Local Joint Engineering Research Center of Safety Technology for Rail Vehicle, Central South University, Changsha, China*
[d]*Department of Mechanical and Aerospace Engineering, Politecnico di Torino, Torino, Italy*

Abstract

In this paper, an exact dynamic stiffness formulation using higher-order theories with displacement variables only is presented and subsequently used to investigate the free vibration characteristics of solid beams, thin-walled structures and reinforced panel structures. In essence, higher-order displacement fields are developed by using the Carrera unified formulation (CUF), and by discretizing the cross-section kinematics with bilinear, cubic and fourth-order Lagrange polynomials. In particular, the component-wise (CW) approach based on Lagrange expansion is applied in which the solid part and thin-walled part are considered as two independent components that can be assembled. The principle of virtual displacements is used to derive the governing differential equations and the associated natural boundary conditions. An exact dynamic stiffness matrix is then developed by relating the amplitudes of harmonically varying loads to those of the responses. The explicit terms of the dynamic stiffness matrices are also presented. The Wittrick–Williams algorithm of the dynamic stiffness method (DSM) is applied with the explicit expressions of the J_0 count for beam elements under all above support conditions. In return, there is no need to refine the element in the DSM, and thus, it becomes immensely efficient. The accuracy and efficiency of the proposed methodology are extensively assessed for different solid beams, thin-walled structures and reinforced panels and the results are compared with those appearing in published literature and also checked by 3D finite element (FE) solutions.

1. Introduction

Beam models are widely used to analyse the mechanical behaviour of slender bodies, such as columns, rotor-blades, aircraft wings, towers, antennae and bridges amongst oth-

---

*Corresponding author. Tel: +86 (0)13873144366
Email addresses: xiaoliu11@csu.edu.cn (Xiao Liu), alfonso.pagani@polito.it (Alfonso Pagani), erasmo.carrera@polito.it (Erasmo Carrera), xiangliu06@gmail.com (Xiang Liu)

ers. Interest in beam models is mainly due to their simplicity and low computational costs when compared to 2D (plate/shell) or 3D (solid) models. The free vibration analysis of beam structures has always been a major area of activity in structural design. The results of modal analyses are, in fact, of great interest in dynamic response analyses, acoustics, aeroelasticity and also to avoid resonance. The classical and well-known beam theories in the free vibration analysis of beam structures are those by Euler [1] and hereinafter referred to as EBBM, and Timoshenko [2, 3] and hereinafter referred to as TBM. The former does not account for transverse shear deformations and rotatory inertia, whereas the latter assumes a uniform shear distribution along the cross-section of the beam together with the effects of rotatory inertia. These models yield reasonably good results when slender, solid section, homogeneous structures are subjected to flexure. Conversely, the analysis of deep, thin-walled, open section beams may require more sophisticated theories to achieve sufficiently accurate results [4]. Therefore, it is necessary to develop a higher-order beam model and an accurate and efficient analysis method for free vibration of beams in engineering applications.

Over the last century, a number of refined beam theories have been developed to overcome the limitations of classical beam modelling. Different approaches have been used to improve the beam models [5–12], which include the introduction of shear correction factors, the use of warping functions based on de Saint-Venant's solution, the variational asymptotic solution (VABS), the generalised beam theory (GBT), and others. A comprehensive review of existing beam theories was published by Kapania and Raciti [5, 6]. Another review of modern theories for beam structures was published by Carrera et al. [7]. As far as the free vibration analysis is concerned, a brief overview about refined 1D models is given here for the sake of completeness. Early researchers have focussed on the use of appropriate shear correction factors to increase the accuracy of classical 1D formulations, notable contributions include the works of Timoshenko and Goodier [8], Sokolniko [13], Stephen [14], and Hutchinson [15]. The shear correction factor has generally been used as a static concept which is restrictive. In this regard, Jensen [16] demonstrated that the shear correction factor can exhibit variations with respect to the natural frequencies. Additionally, a review article by Kaneko [17] and a publication by Dong et al. [18] highlighted the challenges associated with establishing a universally accepted formulation for shear correction factors. Another significant class of refinement methods documented in the literature relies on the utilization of warping functions. Notable contributions in this area include the works of El Fatmi [19–21] and Ladevéze et al. [22, 23]. Rand [24] and Kim and White [25] employed a similar approach in the analysis of free vibration by introducing out-of-plane warping with no in-plane stretching terms. Asymptotic-type expansions in conjunction with variational methods have been proposed, particularly by Berdichevsky et al. [26]. They provide a commendable review of previous works on beam theory developments. Further valuable contributions in this field have been reported by Volovoi [27], Popescu and Hodges [28], and Yu et al. [29–31]. Additional relevant research can be found in the papers published by Kim and Wang [32] and Firouz-Abad et al. [33]. The generalised beam theory (GBT) is believed to have originated from the work of Schardt [34, 35]. GBT improves classical theories by employing a piece-wise beam description for thin-walled sections. It has been widely utilized and further extended in various forms by Silvestre et al. [36–38], with a dynamic application being presented by

Bebiano et al. [39]. Higher-order theories are typically developed by employing refined displacement fields for the beam cross-sections. Washizu [40] demonstrated how the use of a suitably chosen displacement field can lead to closed-form exact 3D solutions. Numerous other higher-order theories have also been proposed to incorporate non-classical effects.

The aforementioned works demonstrate a notable interest in exploring refined beam theories. In contrast to those publications, the Carrera unified formulation (CUF) is a hierarchical formulation that has been well established in the literature for over a decade [41–45]. The strength of CUF lies in its ability to facilitate the automatic development and compact formulation of any structural theory. This is achieved by expressing the 3D displacement field as a series expansion of the generalised unknowns, which are defined along the beam axis in the case of 1D models, through specific cross-sectional functions. A comprehensive discussion about CUF can be found in Carrera's work [41]. Over the past years, the CUF has been applied to different problems by using Taylor expansion (TE) and Lagrange expansion (LE) as cross-sectional functions [46–48]. In the majority of these papers on 1D CUF, the finite element method (FEM) has been used to handle arbitrary geometries and loading conditions. However, the calculation accuracy of the FEM depends heavily on mesh refinement, which in turn restricts the calculation efficiency. In contrast to the 1D Carrera unified formulation (CUF) model solved using weak-form solutions such as FEM, analytical methods are not affected by meshing and can provide highly accurate dynamic analysis. Giunta et al. [49–51] presented a strong-form solution, known as the Navier-type solution, for the 1D CUF TE governing equation. They applied this solution to the free vibration analysis of composite beams [49] as well as the static, buckling, and free vibration analysis of sandwich beams [50, 51]. The extension of the Navier-type closed-form solution to the 1D CUF LE for free vibration analysis of isotropic beams was done by Dan et al. [52]. However, the above analytic method is only limited to the special boundary conditions, e.g., simply supported. It is not easy to develop analytical solutions for the free vibration analysis of beams with solid and thin-walled cross-sections under arbitrary boundary conditions.

A powerful alternative tool has shown great potential for CUF theories through the application of the dynamic stiffness method (DSM) to carry out the free vibration analysis of solid and thin-walled structures in a much broader context by allowing for the cross-sectional deformation. Furthermore, the dynamic stiffness method (DSM) is applicable to beam structures with arbitrary boundary conditions. The DSM is often referred to as an exact method as it is based on the exact general solution of the governing differential equations [53–60]. This essentially means that, unlike the FEM and other approximate methods, the model accuracy is not unduly compromised when a small number of elements are used in the analysis. For instance, one single structural element can be used in the DSM to compute any number of natural frequencies with any desired accuracy. It is worth mentioning that compared to other analytical methods, the DSM applies an efficient and robust algorithm, the Wittrick-Williams (WW) algorithm, which guarantees that no natural frequency is missed. DSM has been quite extensively developed for beam elements by Banerjee et al. [53, 59, 60] and Williams and Wittrick [57, 60]. Liu and his co-authors have proposed DS theories for plate-like structures [61] subjected to general boundary conditions [62, 63], stochastic boundary conditions [64], and beam built-up

structures [65]. Recently, Pagani et al. [66–68] have established an exact dynamic stiffness formulation based on the use of Taylor type polynomials to define the displacement field above the beam cross-section. Each field consists of a direct extension to higher-order expansions of the Timoshenko beam theory. However, the use of Taylor-type expansions has some intrinsic limitations: 1) the introduced variables have a mathematical meaning (derivatives at the beam axes); 2) higher order terms cannot have a local meaning, they can have cross-section properties only; 3) the extension to large rotation formulation could experience difficulties. In addition, the J_0 count in the WW algorithm is an important and difficult problem. J_0 is the number of natural frequencies below the trial frequency when all the nodes of the structure are clamped. Previous researches discretized the structure into a finer dynamic stiffness mesh to ensure that J_0 is equal to zero, which greatly reduces the computational efficiency and does not bring the merit of the DSM into full play.

To overcome these problems, this work combines the dynamic stiffness method (DSM) with beam theories that use Lagrange-type polynomial expansions to describe the displacement field of the cross-section. The use of these expansion functions allows for the representation of displacement variables only. This aspect is particularly advantageous because [46–48]: 1) each variable has a precise physical meaning (the problem unknowns are only translational displacements); 2) unknown variables can be put in fixed zones (sub-domains) of the cross-section area; 3) geometrical boundary conditions can be applied in sub-domains of the cross-section (and not only to the whole cross-section); 4) geometrical boundary conditions can also be applied along the beam-axis; 5) the extension to geometrically non-linear problems appears more suitable than in the case of Taylor-type higher-order theories. In particular, the component-wise (CW) approach based on Lagrange expansion is applied in which the solid part and thin-walled part are considered as two independent components that can be assembled. In the CW approach, each component is modeled individually and simultaneously by using CUF beam elements (see [46]). Then, continuity conditions among the different components are automatically satisfied if Lagrange polynomials are used to approximate the cross-section kinematics. A recent successful application of the CW approach can be seen in [46]. In this work, the Principle of Virtual Displacements (PVD) is used to derive the differential governing equations and the associated natural boundary conditions for the LE model. By assuming harmonic oscillation, the equilibrium equations and the natural boundary conditions are formulated in the frequency domain by making extensive use of symbolic computation. The resulting system of ordinary differential equations of second order with constant coefficients is then solved in a closed analytical form. Subsequently, the frequency-dependent DS matrix of the system is derived by relating the amplitudes of the harmonically varying nodal generalised forces to those of the nodal generalised displacements. Finally, the mode count J_0 of the WW algorithm under support conditions is obtained in this study and extended WW algorithm is applied to the resulting DS matrix for free vibration analysis of solid beams, thin-walled structures and reinforced panel structures. This exact solution for free vibration analysis will be characterized by high efficiency in terms of computational costs and unprecedented accuracy.

The paper is organized as follows: a brief introduction of 1D CUF beam theory is given in Section 2. The governing equations of the LE model and analytical solution are derived using the principle of virtual work in Section 3. Section 4 presents the dynamic

stiffness formulations and extended WW algorithm. Next, three examples taken from the literature are used to validate the proposed model in Section 5, these results are also compared with those from ABAQUS to assess the availability of CUF-DSM to provide 3D accuracy of solid beams, thin-walled structures and reinforced panels under different boundary conditions. Finally, some meaningful conclusions based on the above analysis are obtained in Section 6.

2. 1D CUF LE beam theory

2.1. Preliminaries

The adopted coordinate frame of the generic beam model is presented in Fig.1. The beam has cross-section $\boldsymbol{\Omega}$ and length L. The dimensions along y are $0 \leq y \leq L$. The displacement vector is

$$\mathbf{u}(x, y, z; t) = \left\{ \begin{array}{ccc} u_x & u_y & u_z \end{array} \right\}^T \tag{1}$$

in which u_x, u_y and u_z are the displacement components along x-, y-, z-axes, respectively. The surperscript "T" represents a transpose. The stress, $\boldsymbol{\sigma}$, and the strain, $\boldsymbol{\epsilon}$, components are grouped as follows

$$\boldsymbol{\sigma} = \left\{ \sigma_{yy} \quad \sigma_{xx} \quad \sigma_{zz} \quad \sigma_{xz} \quad \sigma_{yz} \quad \sigma_{xy} \right\}^{\mathrm{T}}, \quad \boldsymbol{\epsilon} = \left\{ \epsilon_{yy} \quad \epsilon_{xx} \quad \epsilon_{zz} \quad \epsilon_{xz} \quad \epsilon_{yz} \quad \epsilon_{xy} \right\}^{\mathrm{T}} \tag{2}$$

In the case of small displacements with respect to a characteristic dimension in the plane of $\boldsymbol{\Omega}$, the strain–displacement relations are

$$\boldsymbol{\epsilon} = \mathbf{D}\mathbf{u} \tag{3}$$

where $\mathbf{D}$ is the following linear differential operator matrix

$$\mathbf{D} = \begin{bmatrix} 0 & \frac{\partial}{\partial y} & 0 \\ \frac{\partial}{\partial x} & 0 & 0 \\ 0 & 0 & \frac{\partial}{\partial z} \\ \frac{\partial}{\partial z} & 0 & \frac{\partial}{\partial x} \\ 0 & \frac{\partial}{\partial z} & \frac{\partial}{\partial y} \\ \frac{\partial}{\partial y} & \frac{\partial}{\partial x} & 0 \end{bmatrix} \tag{4}$$

According to Hooke's law, the relationship between stress and strain is

$$\boldsymbol{\sigma} = \tilde{\mathbf{C}}\boldsymbol{\epsilon} \tag{5}$$

In the case of isotropic material, the matrix $\tilde{\mathbf{C}}$ is

$$\tilde{\mathbf{C}} = \begin{bmatrix} \tilde{C}_{33} & \tilde{C}_{23} & \tilde{C}_{13} & 0 & 0 & 0 \\ \tilde{C}_{23} & \tilde{C}_{22} & \tilde{C}_{12} & 0 & 0 & 0 \\ \tilde{C}_{13} & \tilde{C}_{12} & \tilde{C}_{11} & 0 & 0 & 0 \\ 0 & 0 & 0 & \tilde{C}_{44} & 0 & 0 \\ 0 & 0 & 0 & 0 & \tilde{C}_{55} & 0 \\ 0 & 0 & 0 & 0 & 0 & \tilde{C}_{66} \end{bmatrix} \tag{6}$$
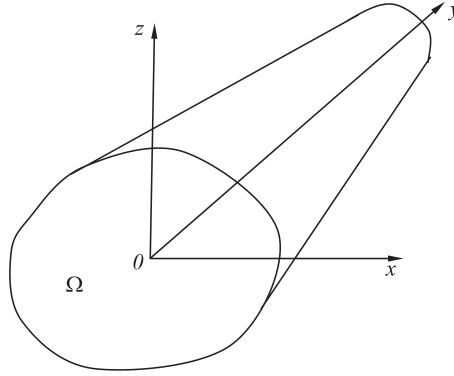
Fig. 1.   Beam model and related Cartesian frame.

Coefficients $\tilde{C}_{ij}$ depend on Young's modulus and Poisson's ratio, which can be found in standard texts, see Reddy [69] or Tsai [70].

2.2. Unified formulation of beams

Within the framework of CUF, the 3D displacement field $\mathbf{u}(x, y, z; t)$ can be expressed as an expansion of the generalised displacements through generic functions F_τ

$$\mathbf{u}(x, y, z; t) = F_\tau(x, z)\mathbf{u}_\tau(y; t), \quad \tau = 1, 2, \ldots, M \tag{7}$$

where F_τ are the functions of the coordinates x and z on the cross-section, $\mathbf{u}_\tau$ is the generalised displacements vector and M stands for the number of terms in the expansion. According to the Einstein notation, the repeated subscript, τ, indicates summation. In this paper, Lagrange polynomials are used for F_τ functions. In particular, 4-point (L4) bilinear, 9-point (L9) cubic and 16-point (L16) fourth-order polynomials are used. The order of the beam model is directly related to the choice of the F_τ cross-sectional polynomial. Refined models of complex structures can also be implemented by considering cross-sectional assembly of those elements, such as in Fig. 2, where one L9 elements in actual geometry are shown. Moreover, the isoparametric formulation is exploited to deal with arbitrary shapes.
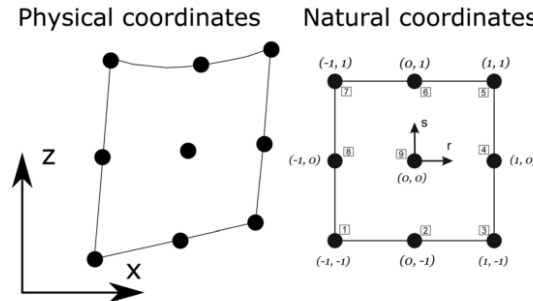

Fig. 2.   Coordinates mapping between coordinate systems.

In the case of the L4 element, the interpolation functions are given by

$$F_\tau = \frac{1}{4}\left(1 + rr_\tau\right)\left(1 + ss_\tau\right), \quad \tau = 1, 2, 3, 4 \tag{8}$$

where r and s are the normalized coordinates that vary from -1 to 1 and r_τ and s_τ are the actual coordinates of the four nodes.

Then, the interpolation functions of 9-point (L9) cubic polynomial element are given by

$$F_\tau = \frac{1}{4}\left(r^2 + rr_\tau\right)\left(s^2 + ss_\tau\right), \quad \tau = 1, 3, 5, 7$$

$$F_\tau = \frac{1}{2}s_\tau^2\left(s^2 + ss_\tau\right)\left(1 - r^2\right) + \frac{1}{2}r_\tau^2\left(r^2 + rr_\tau\right)\left(1 - s^2\right), \quad \tau = 2, 4, 6, 8 \tag{9}$$

$$F_\tau = \left(1 - r^2\right)\left(1 - s^2\right), \quad \tau = 9$$

where r_τ and s_τ are the actual coordinates of the nine nodes.

Finally, the interpolation functions of 16-point (L16) fourth-order polynomial element are given by

$$F_{\tau mn} = L_m(r)L_n(s), \quad m, n = 1, 2, 3, 4 \tag{10}$$

where

$$L_1(r) = \tfrac{1}{16}(r - 1)\left(1 - 9r^2\right), \quad L_2(r) = \tfrac{9}{16}(3r - 1)\left(r^2 - 1\right)$$

$$L_3(r) = \tfrac{9}{16}(3r + 1)\left(1 - r^2\right), \quad L_4(r) = \tfrac{1}{16}(r + 1)\left(9r^2 - 1\right) \tag{11}$$

(a) Two-stringer spar

(b) Each of the two stringers and the panel are modelled with one LE 1D element

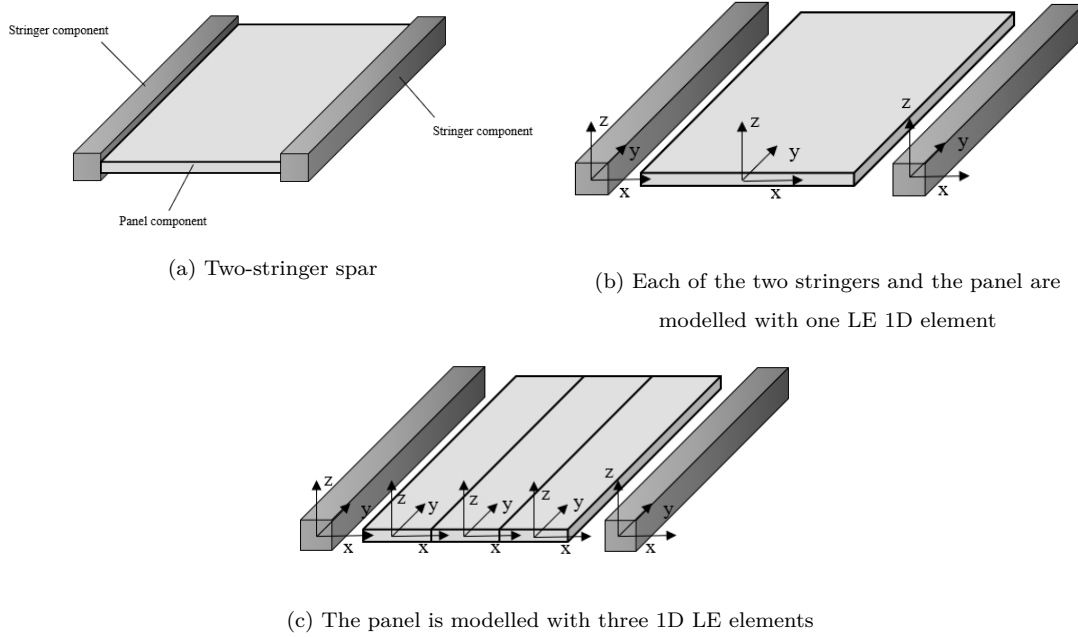(c) The panel is modelled with three 1D LE elements

Fig. 3. Component-wise approach through LE elements.

The cross-section displacement fields can be defined according to different elements and Eq. (7). For instance, the complete displacement field given by one single L4 element is

$$u_x = F_1 u_{x_1} + F_2 u_{x_2} + F_3 u_{x_3} + F_4 u_{x_4}$$

$$u_y = F_1 u_{y_1} + F_2 u_{y_2} + F_3 u_{y_3} + F_4 u_{y_4} \tag{12}$$

$$u_z = F_1 u_{z_1} + F_2 u_{z_2} + F_3 u_{z_3} + F_4 u_{z_4}$$

where u_{x_1}, ..., u_{z_4} are the unknown variables of the problem and represent the translational displacement components of each of the four points of the L4 element. The above displacement variables are the only unknowns, which do not lie on the beam element axis.

As already mentioned, the resulting LE can be used for the whole cross-section or can be introduced by dividing the cross-section into various sub-domains. The resulting approach is referred to as Component-Wise (CW) because Lagrange elements are used to model the displacement variables in each structural component at the cross-sectional level. Fig. 3 shows a possible CW model of the spar where each component is modelled via one 1D LE element. Each LE element is then assembled above the cross-section to obtain the global stiffness matrix based on the 1D formulation. Since panels could not be reasonably modelled via a 1D formulation, 1D CW models can be refined by using several L-elements for one component. This methodology allows us to tune the capabilities of the model by (1) choosing which component requires a more detailed model; (2) setting the order of the structural model to be used.

3. Governing equations of the LE model and analytical solution

The principle of virtual displacements is used to derive the equations of motion

$$\delta L_{\text{int}} = \int_V \delta \boldsymbol{\epsilon}^T \boldsymbol{\sigma} \mathrm{d}V = -\delta L_{\text{ine}} \tag{13}$$

where L_{int} stands for the strain energy and L_{ine} is the work done by the inertial loadings. δ stands for the usual virtual variation operator. The virtual variation of the strain energy is rewritten using Eqs. (3), (6) and (7). After integrations by part, Eq. (13) becomes

$$\delta L_{\text{int}} = \int_L \delta \mathbf{u}_\tau^T \mathbf{K}^{\tau s} \mathbf{u}_s \ \mathrm{d}y + \left[\delta \mathbf{u}_\tau^T \boldsymbol{\Pi}^{\tau s} \mathbf{u}_s \right]_{y=0}^{y=L} \tag{14}$$

where $\mathbf{K}^{\tau s}$ is the linear differential stiffness matrix and $\boldsymbol{\Pi}^{\tau s}$ is the matrix of natural boundary conditions. For the sake of brevity, these matrices are not given here but they can be found in [66–68]. The fundamental nuclei have the key property that their mathematical expressions remain unchanged regardless of the order of the beam theory or the choice of F_τ functions.

The virtual variation of the inertial work is given by

$$\delta L_{\text{ine}} = \int_L \delta \mathbf{u}_\tau \int_\Omega \rho F_\tau F_s \ \mathrm{d}\Omega \ddot{\mathbf{u}}_s \ \mathrm{d}y = \int_L \delta \mathbf{u}_\tau \mathbf{M}^{\tau s} \ddot{\mathbf{u}}_s \ \mathrm{d}y \tag{15}$$

where ρ denotes the material density and double over dots stand for the second derivative with respect to time (t). $\mathbf{M}^{\tau s}$ is the $3{\times}3$ fundamental, diagonal nucleus of the mass matrix,

whose components can be found in [40]. The explicit form of the governing equations is

$$
\begin{aligned}
\delta u_{x\tau} : &- E^{66}_{\tau s} u_{xs,yy} + \left(E^{22}_{\tau,x s,x} + E^{44}_{\tau,z s,z} \right) u_{xs} + \left(E^{23}_{\tau,x s} - E^{66}_{\tau s,x} \right) u_{ys,y} \\
&+ \left(E^{44}_{\tau,z s,x} + E^{12}_{\tau,x s,z} \right) u_{zs} = -E^{\rho}_{\tau s} \ddot{u}_{xs} \\
\delta u_{y\tau} : &\left(E^{66}_{\tau,x s} - E^{23}_{\tau s,x} \right) u_{xs,y} - E^{33}_{\tau s} u_{ys,yy} + \left(E^{66}_{\tau,x s,x} + E^{55}_{\tau,z s,z} \right) u_{ys} \\
&+ \left(E^{55}_{\tau,z s} - E^{13}_{\tau s,z} \right) u_{zs,y} = -E^{\rho}_{\tau s} \ddot{u}_{ys} \\
\delta u_{z\tau} : &\left(E^{44}_{\tau,x s,z} + E^{12}_{\tau,z s,x} \right) u_{xs} + \left(E^{13}_{\tau,z s} - E^{55}_{\tau s,z} \right) u_{ys,y} - E^{55}_{\tau s} u_{zs,yy} \\
&+ \left(E^{44}_{\tau,x s,x} + E^{11}_{\tau,z s,z} \right) u_{zs} = -E^{\rho}_{\tau s} \ddot{u}_{zs}
\end{aligned}
\tag{16}
$$

The generic term $E^{\alpha\beta}_{\tau,\theta s,\zeta}$ above is a cross-sectional moment parameter

$$
E^{\alpha\beta}_{\tau,\theta s,\zeta} = \int_{\Omega} \tilde{C}_{\alpha\beta} F_{\tau,\theta} F_{s,\zeta} \, d\Omega
\tag{17}
$$

The suffix after the comma denotes the derivatives. Moreover,

$$
E^{\rho}_{\tau s} = \int_{\Omega} \rho F_{\tau} F_s \, d\Omega
\tag{18}
$$

Letting $\mathbf{P}_\tau = \{ P_{x\tau} \quad P_{y\tau} \quad P_{z\tau} \}^T$ to be the vector of the generalised forces, the natural boundary conditions are

$$
\begin{aligned}
\delta u_{x\tau} : P_{xs} &= E^{66}_{\tau s} u_{xs,y} + E^{66}_{\tau s,x} u_{ys} \\
\delta u_{y\tau} : P_{ys} &= E^{23}_{\tau s,x} u_{xs} + E^{33}_{\tau s} u_{ys,y} + E^{13}_{\tau s,z} u_{zs} \\
\delta u_{z\tau} : P_{zs} &= E^{55}_{\tau s,z} u_{ys} + E^{55}_{\tau s} u_{zs,y}
\end{aligned}
\tag{19}
$$

For a fixed approximation order, Eqs. (16) and (19) have to be expanded using the indices τ and s in order to obtain the governing differential equations and the natural boundary conditions of the desired model. In the case of harmonic motion, the solution of Eq. (16) is sought in the form

$$
\mathbf{u}_s(y;t) = \mathbf{U}_s(y) e^{i\omega t}
\tag{20}
$$

where $\mathbf{U}_s(y)$ is the amplitude function of the motion, ω is an arbitrary circular or angular frequency, and i is the imaginary unit. Eq. (20) allows the formulation of the equilibrium equations and the natural boundary conditions in the frequency domain. Substituting Eq. (20) into Eq. (16), a set of three coupled ordinary differential equations is obtained which can be written in a matrix form as follows

$$
\delta \mathbf{U}_\tau : \mathbf{L}^{\tau s} \tilde{\mathbf{U}}_s = 0
\tag{21}
$$

where

$$
\tilde{\mathbf{U}}_s = \{ U_{xs} \quad U_{xs,y} \quad U_{xs,yy} \quad U_{ys} \quad U_{ys,y} \quad U_{ys,yy} \quad U_{zs} \quad U_{zs,y} \quad U_{zs,yy} \}^T
\tag{22}
$$

$\mathbf{L}^{\tau s}$ is the 3×9 fundamental nucleus of the matrix containing the coefficients of the ordinary differential equations. For the sake of brevity, the explicit expressions concerning
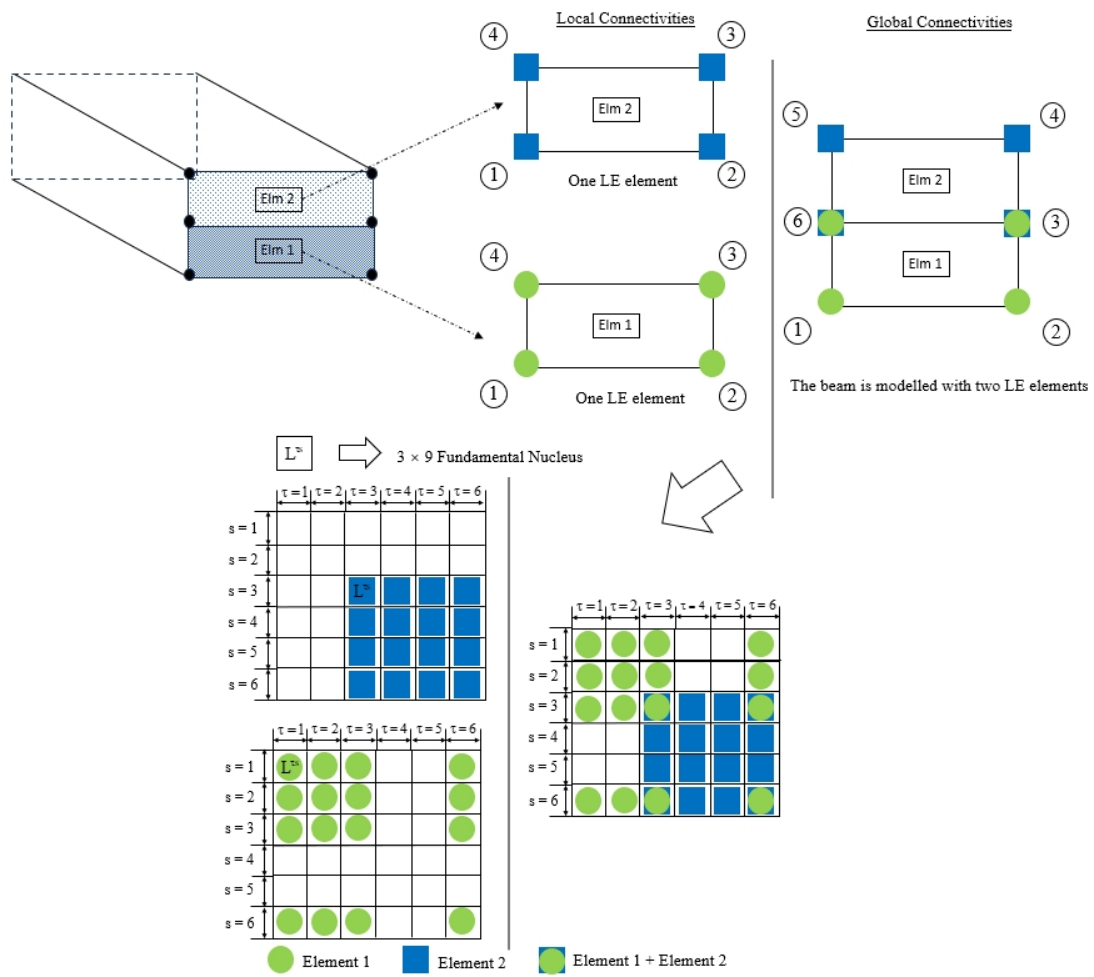
Fig. 4.   Expansion of the matrix $\mathbf{L}^{\tau s}$ for two L4 elements assembls within a beam node.

these fundamental nuclei are not reported here, but are available from the corresponding literature [67, 68].

The equations of motion can be obtained in the form of Eq. (23) as given below by expanding $\mathbf{L}^{\tau s}$ as shown in Figs. 4. It reads as

$$\mathbf{L}\tilde{\mathbf{U}} = 0 \tag{23}$$

In a similar way, the boundary conditions of Eq. (19) can be written in a matrix form as

$$\delta \mathbf{U}_\tau : \mathbf{P}_s = \mathbf{B}^{\tau s}\hat{\mathbf{U}}_s \tag{24}$$

where

$$\hat{\mathbf{U}}_s = \{U_{xs} \quad U_{xs,y} \quad U_{ys} \quad U_{ys,y} \quad U_{zs} \quad U_{zs,y}\}^{\mathrm{T}} \tag{25}$$

and $\mathbf{B}^{\tau s}$ is the 3×6 fundamental nucleus which contains the coefficients of the natural boundary conditions which are available from the corresponding literature [67, 68]. For a given expansion order, the natural boundary conditions can be obtained in the form of Eq. (26) by expanding $\mathbf{B}^{\tau s}$ in the same way as $\mathbf{L}^{\tau s}$ to finally give

$$\mathbf{P} = \mathbf{B}\hat{\mathbf{U}} \tag{26}$$

Eq. (23) is a system of ordinary differential equations (ODEs) of second order in y with constant coefficients. A change of variables is used to reduce the second order system of ODEs to a first order system.

$$\begin{aligned}
\mathbf{Z} &= \{Z_1 \quad Z_2 \quad \dots \quad Z_n\}^T = \hat{\mathbf{U}} \\
&= \{ U_{x1} \quad U_{x1,y} \quad U_{y1} \quad U_{y1,y} \quad U_{z1} \quad U_{z1,y} \quad \dots \quad U_{xM} \quad U_{xM,y} \quad U_{yM} \\
&\quad U_{yM,y} \quad U_{zM} \quad U_{zM,y} \}^T
\end{aligned} \tag{27}$$

where $\hat{\mathbf{U}}$ is the expansion of $\hat{\mathbf{U}}_s$ for a given theory order, M is the number of expansion terms for the given DSM-LE theory, and $n = 6 \times M$ is the dimension of the unknown vector as well as the number of differential equations. In [67], an automatic algorithm to transform the $\mathbf{L}$ matrix of Eq. (23) into the matrix $\mathbf{S}$ of the following linear differential system was described

$$\mathbf{Z}_{,y}(y) = \mathbf{S}\mathbf{Z}(y) \tag{28}$$

Once the differential problem is described in terms of Eq. (28), the solution can be written as follows

$$\begin{bmatrix} Z_1 \\ Z_2 \\ \vdots \\ Z_n \end{bmatrix} = \begin{bmatrix} \delta_{11} & \delta_{21} & \dots & \delta_{n1} \\ \delta_{12} & \delta_{22} & \dots & \delta_{n2} \\ \vdots & \vdots & \ddots & \vdots \\ \delta_{1n} & \delta_{2n} & \dots & \delta_{nn} \end{bmatrix} \begin{bmatrix} C_1 \mathrm{e}^{\lambda_1 y} \\ C_2 \mathrm{e}^{\lambda_2 y} \\ \vdots \\ C_n \mathrm{e}^{\lambda_n y} \end{bmatrix} \tag{29}$$

where λ_i is the i-th eigenvalue of the $\mathbf{S}$ matrix, δ_{ij} is the j-th element of the i-th eigenvector of the $\mathbf{S}$ matrix and C_i are the integration constants which need to be determined by using the boundary conditions. The above equation can be written in matrix form as follows

$$\mathbf{Z} = \delta \mathbf{C} e^{\lambda y} \tag{30}$$

Vector $\mathbf{Z}$ does not only contain the displacements but also their first derivatives. If only the displacements are needed, according to Eq. (27), only the lines 1, 3, 5, $\cdots$, $n-1$ should be taken into account, giving a solution in the following form

$$
\begin{aligned}
U_{x1}(y) &= C_1\delta_{11}\mathrm{e}^{\lambda_1 y} + C_2\delta_{21}\mathrm{e}^{\lambda_2 y} + \ldots + C_n\delta_{n1}\mathrm{e}^{\lambda_n y} \\
U_{y1}(y) &= C_1\delta_{13}\mathrm{e}^{\lambda_1 y} + C_2\delta_{23}\mathrm{e}^{\lambda_2 y} + \ldots + C_n\delta_{n3}\mathrm{e}^{\lambda_n y} \\
U_{z1}(y) &= C_1\delta_{15}\mathrm{e}^{\lambda_1 y} + C_2\delta_{25}\mathrm{e}^{\lambda_2 y} + \ldots + C_n\delta_{n5}\mathrm{e}^{\lambda_n y} \\
&\vdots \\
U_{zM}(y) &= C_1\delta_{1(n-1)}\mathrm{e}^{\lambda_1 y} + C_2\delta_{2(n-1)}\mathrm{e}^{\lambda_2 y} + \ldots + C_n\delta_{n(n-1)}\mathrm{e}^{\lambda_n y}
\end{aligned} \tag{31}
$$

Once the displacements are known, the boundary conditions are obtained by substituting the solution of Eq. (30) into the boundary conditions (Eq. (26)). In fact, it should be noted that $\hat{\mathbf{U}}$ is equal to $\mathbf{Z}$ (Eq. (27)). It reads

$$\mathbf{P} = \mathbf{B}\delta \mathbf{C} e^{\lambda y} = \mathbf{\Lambda} \mathbf{C} e^{\lambda y} \tag{32}$$

where $\mathbf{\Lambda} = \mathbf{B}\delta$. The boundary conditions can be written in explicit form as follows

$$
\begin{aligned}
P_{x1}(y) &= C_1\Lambda_{11}\mathrm{e}^{\lambda_1 y} + C_2\Lambda_{12}\mathrm{e}^{\lambda_2 y} + \ldots + C_n\Lambda_{1n}\mathrm{e}^{\lambda_n y} \\
P_{y1}(y) &= C_1\Lambda_{21}\mathrm{e}^{\lambda_1 y} + C_2\Lambda_{22}\mathrm{e}^{\lambda_2 y} + \ldots + C_n\Lambda_{2n}\mathrm{e}^{\lambda_n y} \\
P_{z1}(y) &= C_1\Lambda_{31}\mathrm{e}^{\lambda_1 y} + C_2\Lambda_{32}\mathrm{e}^{\lambda_2 y} + \ldots + C_n\Lambda_{3n}\mathrm{e}^{\lambda_n y} \\
&\vdots \\
P_{zM}(y) &= C_1\Lambda_{n1}\mathrm{e}^{\lambda_1 y} + C_2\Lambda_{n2}\mathrm{e}^{\lambda_2 y} + \ldots + C_n\Lambda_{nn}\mathrm{e}^{\lambda_n y}
\end{aligned} \tag{33}
$$

4. The dynamic stiffness formulation

4.1. Dynamic stiffness matrix

Once the closed form analytical solution of the differential equations of motion of the structural element in free vibration has been sought, a number of general boundary conditions which are usually the nodal displacements and forces - equal to twice the number of integration constants in algebraic form needs to be applied (see Fig. 5).

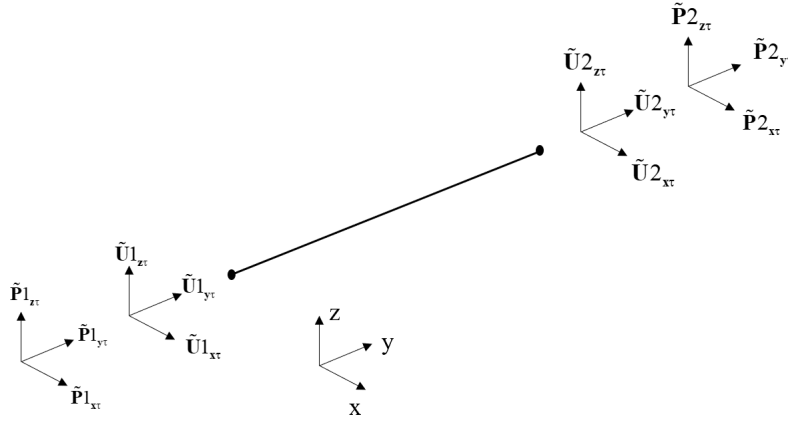Starting from the displacements, the boundary conditions can be written as

Fig. 5.   Boundary conditions of the beam element and sign conventions.

$$
\begin{aligned}
y = 0: &\qquad\qquad y = L: \\
U_{x1}(0) = \bar{U}1_{x1} &\qquad\qquad U_{x1}(L) = \bar{U}2_{x1} \\
U_{y1}(0) = \bar{U}1_{y1} &\qquad\qquad U_{y1}(L) = \bar{U}2_{y1} \\
U_{z1}(0) = \bar{U}1_{z1} &\qquad\qquad U_{z1}(L) = \bar{U}2_{z1} \\
\vdots &\qquad\qquad\quad \vdots \\
U_{zM}(0) = \bar{U}1_{zM} &\qquad\qquad U_{zM}(L) = \bar{U}2_{zM}
\end{aligned}
\tag{34}
$$

By evaluating Eq. (31) at $y = 0$ and $y = L$ and applying the boundary conditions of Eq. (34), the following matrix relation for the nodal displacements is obtained

$$
\begin{Bmatrix}
\bar{U}1_{x1} \\
\bar{U}1_{y1} \\
\bar{U}1_{z1} \\
\vdots \\
\bar{U}1_{zM} \\
\bar{U}2_{x1} \\
\bar{U}2_{y1} \\
\bar{U}2_{z1} \\
\vdots \\
\bar{U}2_{zM}
\end{Bmatrix}
=
\begin{bmatrix}
\delta_{11} & \delta_{21} & \dots & \delta_{n1} \\
\delta_{13} & \delta_{23} & \dots & \delta_{n3} \\
\delta_{15} & \delta_{25} & \dots & \delta_{n5} \\
\vdots & \vdots & \ddots & \vdots \\
\delta_{1(n-1)} & \delta_{2(n-1)} & \dots & \delta_{n(n-1)} \\
\delta_{11}e^{\lambda_1 L} & \delta_{21}e^{\lambda_2 L} & \dots & \delta_{n1}e^{\lambda_n L} \\
\delta_{13}e^{\lambda_1 L} & \delta_{23}e^{\lambda_2 L} & \dots & \delta_{n3}e^{\lambda_n L} \\
\delta_{15}e^{\lambda_1 L} & \delta_{25}e^{\lambda_2 L} & \dots & \delta_{n5}e^{\lambda_n L} \\
\vdots & \vdots & \ddots & \vdots \\
\delta_{1(n-1)}e^{\lambda_1 L} & \delta_{2(n-1)}e^{\lambda_2 L} & \dots & \delta_{n(n-1)}e^{\lambda_n L}
\end{bmatrix}
\begin{Bmatrix}
C_1 \\
C_2 \\
C_3 \\
\vdots \\
C_{\frac{n}{2}} \\
C_{\frac{n}{2}+1} \\
C_{\frac{n}{2}+2} \\
C_{\frac{n}{2}+3} \\
\vdots \\
C_n
\end{Bmatrix}
\tag{35}
$$

The above equation can be written in a more compact form as

$$
\overline{\mathbf{U}} = \mathbf{AC}
\tag{36}
$$

Similarly, boundary conditions for generalised nodal forces are as follows

$$
\begin{aligned}
&y = 0 && y = L: \\
&P_{x1}(0) = -\bar{P}1_{x1} && P_{x1}(L) = \bar{P}2_{x1} \\
&P_{y1}(0) = -\bar{P}1_{y1} && P_{y1}(L) = \bar{P}2_{y1} \\
&P_{z1}(0) = -\bar{P}1_{z1} && P_{z1}(L) = \bar{P}2_{z1} \\
&\vdots && \vdots \\
&P_{zM}(0) = -\bar{P}1_{zM} && P_{zM}(L) = \bar{P}2_{zM}
\end{aligned}
\tag{37}
$$

By evaluating Eq. (33) at $y = 0$ and $y = L$ and applying the BCs of Eq. (37), the following matrix relation for the nodal forces is obtained

$$
\left\{
\begin{array}{c}
\bar{P}1_{x1} \\
\bar{P}1_{y1} \\
\bar{P}1_{z1} \\
\vdots \\
\bar{P}1_{zM} \\
\bar{P}2_{x1} \\
\bar{P}2_{y1} \\
\bar{P}2_{z1} \\
\vdots \\
\bar{P}2_{zM}
\end{array}
\right\}
=
\left[
\begin{array}{cccc}
-\Lambda_{11} & -\Lambda_{12} & \dots & -\Lambda_{1n} \\
-\Lambda_{21} & -\Lambda_{22} & \dots & -\Lambda_{2n} \\
-\Lambda_{31} & -\Lambda_{32} & \dots & -\Lambda_{3n} \\
\vdots & \vdots & \ddots & \vdots \\
-\Lambda_{n1} & -\Lambda_{n2} & \dots & -\Lambda_{nn} \\
\Lambda_{11}e^{\lambda_1 L} & \Lambda_{12}e^{\lambda_2 L} & \dots & \Lambda_{1n}e^{\lambda_n L} \\
\Lambda_{21}e^{\lambda_1 L} & \Lambda_{22}e^{\lambda_2 L} & \dots & \Lambda_{2n}e^{\lambda_n L} \\
\Lambda_{31}e^{\lambda_1 L} & \Lambda_{32}e^{\lambda_2 L} & \dots & \Lambda_{3n}e^{\lambda_n L} \\
\vdots & \vdots & \ddots & \vdots \\
\Lambda_{n1}e^{\lambda_1 L} & \Lambda_{n2}e^{\lambda_2 L} & \dots & \Lambda_{nn}e^{\lambda_n L}
\end{array}
\right]
\left\{
\begin{array}{c}
C_1 \\
C_2 \\
C_3 \\
\vdots \\
C_{\frac{n}{2}} \\
C_{\frac{n}{2}+1} \\
C_{\frac{n}{2}+2} \\
C_{\frac{n}{2}+3} \\
\vdots \\
C_n
\end{array}
\right\}
\tag{38}
$$

The above equation can be written in a more compact form as

$$
\overline{\mathbf{P}} = \mathbf{R}\mathbf{C} \tag{39}
$$

The integration constants vector $\mathbf{C}$ from Eqs. (36) and (39) can now be eliminated by relating the harmonically varying amplitudes of the generalised nodal forces to the corresponding generalised displacements to give the DS matrix of one beam element as follows

$$
\overline{\mathbf{P}} = \mathbf{K}\overline{\mathbf{U}} \tag{40}
$$

where

$$
\mathbf{K} = \mathbf{R}\mathbf{A}^{-1} \tag{41}
$$

$\mathbf{K}$ is the required DS matrix. The DS matrix given by Eq. (41) is the basic building block to compute the exact natural frequencies of a higher-order beam. The global DS matrix can be obtained by assembling elemental matrices as in the classical way of FEM [61]. In particular, it is possible to assemble elemental DS matrices to form the overall DS matrix of any complex structures consisting of beam elements (see Fig. 6).

The global DS matrix can be written as

$$
\overline{\mathbf{P}}^G = \mathbf{K}^G \overline{\mathbf{U}}^G \tag{42}
$$

where $\mathbf{K}^G$ is the square global DS matrix of the final structure. For the sake of simplicity, the subscript "G" is omitted hereafter. The boundary conditions can be applied by simply removing rows and columns of the stiffness matrix corresponding to the degrees of freedom
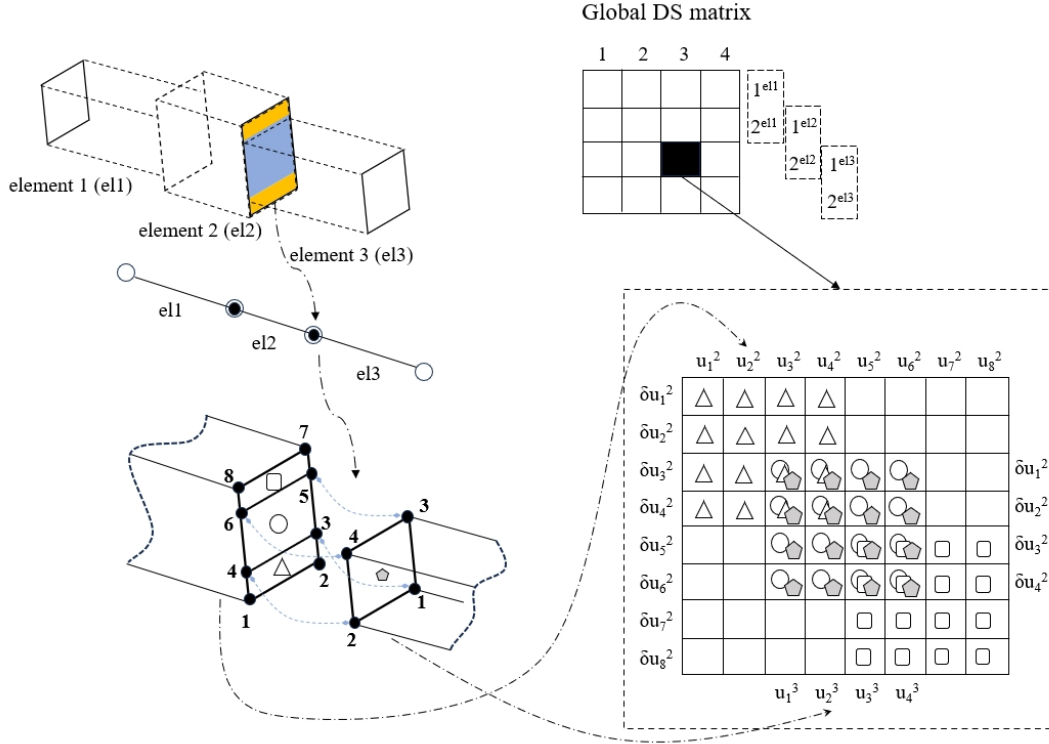
Fig. 6. Assembly of dynamic stiffness matrices of a beam with different cross-sections.

which are zeroes. Due to the presence of degrees of freedom at each interface, a multitude of boundary conditions can be applied at the required nodes.

4.2. The extended Wittrick–Williams algorithm and mode shapes computation

Once the dynamic stiffness matrix is developed, the Wittrick–Williams algorithm can be applied to compute the natural frequencies ω of structures. The following equation is the key equation of the Wittrick–Williams algorithm, which is used to calculate the mode count J when ω is lower than the trial frequency ω^*

$$J = J_0 + s\left(\mathbf{K}(\omega^*)\right) \tag{43}$$

where $\mathbf{K}(\omega^*)$ is the elemental dynamic stiffness matrix, $s(\mathbf{K}(\omega^*)$ is the number of negative diagonal elements after upper triangular transformation by using Gauss elimination of $\mathbf{K}(\omega^*)$, and J_0 is the number of natural frequencies between $\omega = 0$ and $\omega = \omega^*$ when the nodal boundaries of the beam element are fully clamped. There is no doubt that J_0 plays an important role in the Wittrick–Williams algorithm. However, calculating J_0 is generally a difficult problem, and the traditional way is to refine the mesh to make sure $J_0 = 0$. Obviously, it will introduce unnecessary computational cost significantly.

In this study, the J_0 problem of the beam element is resolved by applying an indirect method, it improves the computational efficiency of the dynamic stiffness method. According to the Wittrick–Williams algorithm, the mode count J_s of the beam element with all simply supported (SS) when the half-wave number in the y direction is m can be

given by Eq. (43), which can be recast as

$$J_0 = \sum_1^m J_{0m} \tag{44}$$

$$J_{0m} = J_{sm} - s\left(\mathbf{K}^s(\omega^*)\right) \tag{45}$$

where J_{0m} is J_0 when the half-wave number in the y direction is m and $\mathbf{K}^s(\omega^*)$ is the dynamic stiffness matrix $\mathbf{K}(\omega^*)$ for a beam element with all simply supported when m is a certain value. The detailed solution process for J_{sm} is given as follows: The first step is to solve the natural frequencies ω^S of the beam element under certain m for SS boundary conditions. Consider the BC of the beam element is SS, the displacement fields are assumed as a sum of harmonic functions

$$
\begin{aligned}
u_{x\tau}(y;t) &= U_{x\tau} e^{i\omega t} \sin(\alpha y) \\
u_{y\tau}(y;t) &= U_{y\tau} e^{i\omega t} \cos(\alpha y) \\
u_{z\tau}(y;t) &= U_{z\tau} e^{i\omega t} \sin(\alpha y)
\end{aligned}
\tag{46}
$$

where α is

$$\alpha = \frac{m\pi}{L} \tag{47}$$

By substituting Eq. (46) into the Eq. (16), it holds

$$
\begin{aligned}
\delta U_{x\tau} : &\left(\alpha^2 E_{\tau s}^{66} + E_{\tau,x s,x}^{22} + E_{\tau,z s,z}^{44} - \omega^2 E_{\tau s}^{\rho}\right) U_{xs} \\
&- \alpha\left(E_{\tau,x s}^{23} - E_{\tau s,x}^{66}\right) U_{ys} + \left(E_{\tau,z s,x}^{44} + E_{\tau,x s,z}^{12}\right) U_{zs} = 0 \\
\delta U_{y\tau} : &\quad \alpha\left(E_{\tau,x s}^{66} - E_{\tau s,x}^{23}\right) U_{xs} + \left(\alpha^2 E_{\tau s}^{33} + E_{\tau,z s,x}^{66} + E_{\tau,z s,z}^{55}\right. \\
&\left. -\omega^2 E_{\tau s}^{\rho}\right) U_{ys} + \alpha\left(E_{\tau,z s}^{55} - E_{\tau s,z}^{13}\right) U_{zs} = 0 \\
\delta U_{z\tau} : &\left(E_{\tau,x s,z}^{44} + E_{\tau,z s,x}^{12}\right) U_{xs} - \alpha\left(E_{\tau,z s}^{13} - E_{\tau s,z}^{55}\right) U_{ys} + \left(\alpha^2 E_{\tau s}^{55}\right. \\
&\left. + E_{\tau,x s,x}^{44} + E_{\tau,z s,z}^{11} - \omega^2 E_{\tau s}^{\rho}\right) U_{zs} = 0
\end{aligned}
\tag{48}
$$

The above equations can be converted into the algebraic eigensystem as

$$(\overline{\mathbf{K}}^S - \omega^2 \overline{\mathbf{M}}^S)\overline{\mathbf{U}} = 0 \tag{49}$$

where $\overline{\mathbf{K}}^S$ and $\overline{\mathbf{M}}^S$ are the fundamental nuclei of the algebraic stiffness and mass matrices, respectively. The components of the linear stiffness matrix $\overline{\mathbf{K}}^S$ are

$$
\overline{\mathbf{K}}^S = \begin{bmatrix}
\left(\alpha^2 E_{\tau s}^{66} + E_{\tau,x s,x}^{22} + E_{\tau,z s,z}^{44}\right) & -\alpha\left(E_{\tau,x s}^{23} - E_{\tau s,x}^{66}\right) & \left(E_{\tau,z s,x}^{44} + E_{\tau,x s,z}^{12}\right) \\
\alpha\left(E_{\tau,x s}^{66} - E_{\tau s,x}^{23}\right) & \alpha^2 E_{\tau s}^{33} + E_{\tau,x s,x}^{66} + E_{\tau,z s,z}^{55} & \alpha\left(E_{\tau,z s}^{55} - E_{\tau s,z}^{13}\right) \\
\left(E_{\tau,x s,z}^{44} + E_{\tau,z s,x}^{12}\right) & -\alpha\left(E_{\tau,z s}^{13} - E_{\tau s,z}^{55}\right) & \alpha^2 E_{\tau s}^{55} + E_{\tau,x s,x}^{44} + E_{\tau,z s,z}^{11}
\end{bmatrix}
\tag{50}
$$

The components of the linear mass matrix $\overline{\mathbf{M}}^S$ are

$$\overline{\mathbf{M}}^S = \begin{bmatrix} E^\rho_{\tau s} & 0 & 0 \\ 0 & E^\rho_{\tau s} & 0 \\ 0 & 0 & E^\rho_{\tau s} \end{bmatrix} \tag{51}$$

Once the natural frequencies ω^S of the beam element under certain m for SS boundary conditions are computed, J_{sm} is equal to the number of these frequencies ω^S that are lower than the trial frequency ω^*. Finally, through Eqs. (43), (44) and (45), the natural frequency of the beam under different boundary conditions can be calculated accurately and efficiently. After computing the natural frequency and evaluating the global dynamic stiffness (DS) matrix, the corresponding nodal generalized displacements can be determined by solving the associated homogeneous system of Eq. (42). By utilizing the nodal generalized displacements $\overline{\mathbf{U}}$, the integration constants $\mathbf{C}$ of the element can be calculated using Eq. (36). Subsequently, employing Eq. (31), the unknown generalized displacements can be obtained as a function of y. Finally, by employing Eqs. (1) and (20), the complete displacement field can be generated as a function of x, y, z, and time t (if an animated plot is required). The plot of the desired mode and element can be visualized on a fictitious 3D mesh.

5. Numerical results

The accuracy and computational efficiency of the present approach are demonstrate by carrying out the free vibration analysis of both solid and thin-walled structures in this section. In Section 5.1, free vibration of beams with rectangular cross-section are addressed so as to make an easy and straightforward comparisons with classical beam theories, CUF(TE)-DSM, CUF(LE)-Navier theory and reference FE results. In Section 5.2, a thin-walled C-shaped cross-section beam is considered. Free vibration analysis is carried out for different BCs and the present CUF(LE)-DSM models are also compared with reference solutions from the literature together with the results obtained from the FE commercial software ABAQUS.

5.1. Solid beam structures

A beam with a solid rectangular cross-section are considered for preliminary assessments. The LE cross-sectional discretizations with Lagrange elements are depicted in Fig. 7 for the problem under consideration. Unless differently specified, "1" in "1 × 2L4" stands for the number of L4 elements along the ox direction, and "2" is the number of L4 elements along the oz direction. The beam has a square cross-section ($a = b$), with $b = 0.2$ m. A slenderness rotios L/b equal to 10. The isotropic material datas are: Young modulus, $E = 75$GPa, Poisson ratio, $\nu = 0.33$, material density, $\rho = 2700$ kg/m^3.

Table 1 shows the first seven non-dimensional flexural frequencies $\omega^* = (\omega L^2/b)\sqrt{\rho/E}$ for the simply supported (SS) square beam with $L/b = 10$. The results from the present LE models are compared to those from classical theories (EBBM, TBM), CUF(TE)-DSM, CUF(LE)-Navier theory and reference FE results from Ref. [52, 67]. Various LE models are considered in the table as shown in Fig. 7. The comparison of the results in Table 1 shows the correctness of the present strong form LE beam. Even the most simple one, 1L4, demonstrates its convergence with respect to EBBM. The results obtained by the
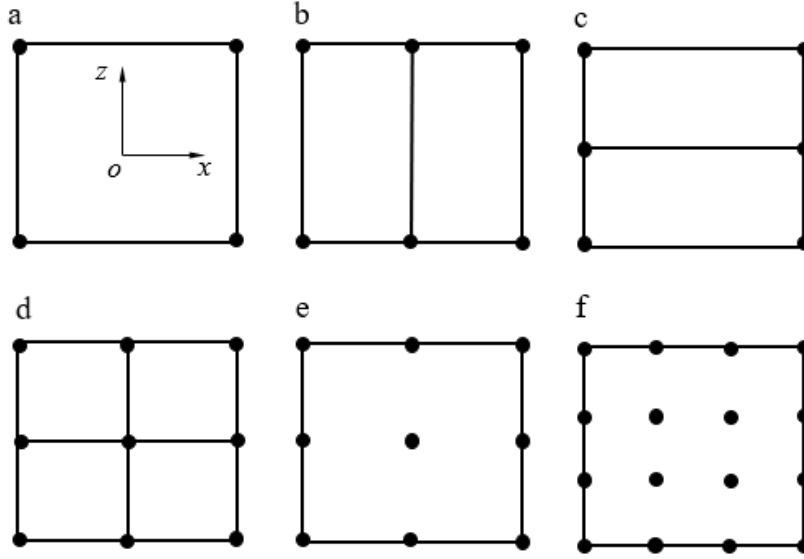
Fig. 7. LE modelling of the square cross-section beam. (a) 1L4. (b) 1×2L4. (c) 2×1L4. (d) 2×2L4. (e) 1L9. (f) 1L16.

Table 1. First seven non-dimensional flexural frequencies $\omega^* = (\omega L^2/b)\sqrt{\rho/E}$ for the simply supported (SS) square beam, $L/b = 10$

Model	1	2	3	4	5	6	7
TBM-DSM [67]	2.807	10.779	22.849	37.858	54.856	73.192	92.334
EBBM-DSM [67]	2.838	11.213	24.742	42.847	64.869	90.330	117.859
FEM [67]							
$NAS1D_{50}$	2.813	10.841	23.055	38.225	55.256	73.331	91.907
$NAS1D_{100}$	2.813	10.841	23.060	38.246	55.323	73.491	92.225
$NAS1D_{200}$	2.813	10.842	23.062	38.254	55.340	73.532	92.296
CUF (TE)-DSM [67]							
N=3	2.803	10.723	22.621	37.299	53.812	71.509	89.963
N=4	2.803	10.722	22.617	37.282	53.765	71.402	89.759
CUF (LE)-Navier [52]							
1L4	3.063	11.704	24.653	40.573	58.415	77.456	97.226
1×2L4	2.914	11.168	23.617	39.030	56.416	75.074	94.536
2×1L4	2.998	11.474	24.213	39.923	57.575	76.452	96.083
2×2L4	2.839	10.890	23.055	38.143	55.187	73.500	92.621
1L9	2.808	10.784	22.869	37.902	54.929	73.268	92.453
1L16	2.803	10.722	22.618	37.291	53.794	71.472	89.898
Current theory							
1L4	3.063	11.704	24.653	40.573	58.415	77.456	97.226
1×2L4	2.914	11.168	23.617	39.030	56.416	75.074	94.536
2×1L4	2.998	11.474	24.213	39.923	57.575	76.452	96.083
2×2L4	2.839	10.890	23.055	38.143	55.187	73.500	92.621
1L9	2.808	10.784	22.869	37.902	54.929	73.268	92.453
1L16	2.803	10.722	22.618	37.291	53.794	71.472	89.898

present method are in good agreement with the Navier solution which also uses LE model. Attention should be paid to $1 \times 2L4$ and $2 \times 1L4$, which are different models, and thus presenting different behavior in the flexure directions along ox and oz. Though the $2 \times 2L4$ model of Fig. 7(d) has the same number of DOFs as 1L9, the latter presents slightly more precise results, at least in the range of the lower frequencies. The results of the 16L9 model show the higher-interpolation, fourth-order capabilities, owning the best accuracy, which is particularly evident in the higher frequencies range.
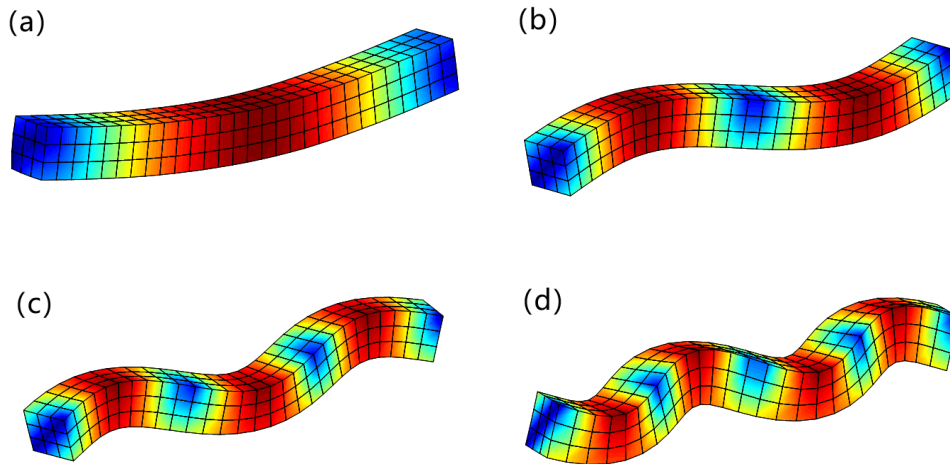

Fig. 8. First (a), second (b) , third (c) and forth (d) flexural modes for a SS square beam ($L = b \times 10$), L9.

Fig. 8 shows the first four flexural modes of the beam with SS boundary conditions obtained from the CUF-DSM analysis when using a 1L9 LE model. It should be emphasised that DSM results are mesh independent and the mesh used in Fig. 8 is merely a plotting grid for convenience. Those figures clearly demonstrate the 3D capabilities of the present CUF-DSM beam formulation.

One of the most important features of the DSM is that it provides exact solutions for any kind of boundary conditions. Moreover, LE theories are able to take into account several non-classical effects such as warping, in-plane deformations, shear effects and flexural-torsion couplings. Table 2 shows the first two flexural modes and the first two torsional modes for a clamped–free (CF) square beam for $L/b = 10$. The exact solutions for classical, linear and higher-order beam theories are also shown and they were computed using the DSM [67]. The CUF(TE)-DSM and reference FE results were computed from Ref. [67]. It can be seen that the present simple one (1L4) LE model is able to characterise the flexural behaviour of solid cross-section beams. A higher-interpolation (1L16) LE model is necessary to correctly detect torsional frequencies.

Fig. 9 shows some representative modal shapes for the 1L9 LE model of the CF beam. Those figures also demonstrate the 3D capabilities of the present CUF-DSM beam formulation for both flexural and torsional modes with any kind of boundary conditions.

Table 2. Non-dimensional natural frequencies $\omega^* = (\omega L^2/b)\sqrt{\rho/E}$ for the CF square beam, $L/b = 10$

Model	I Flexural	II Flexural	I Torsional	II Torsional
TBM-DSM [67]	1.008	6.069	-[a]	-[a]
EBBM-DSM [67]	1.013	6.276	-[a]	-[a]
FEM [67]				
$NAS3D_{12}$	1.021	6.117	8.822	26.318
$NAS3D_{24}$	1.016	6.088	8.852	26.516
CUF (TE)-DSM [67]				
N=3	1.014	6.075	9.631	28.893
N=4	1.013	6.070	8.871	26.619
N=5	1.013	6.069	8.868	26.603
Current theory				
1L4	1.107	6.626	9.631	28.894
1×2L4	1.052	6.319	9.631	28.894
2×1L4	1.052	6.319	9.631	28.894
2×2L4	1.039	6.246	9.631	28.894
1L9	1.015	6.106	9.631	28.893
1L16	1.013	6.073	8.870	26.612

[a] Not provided by the model.

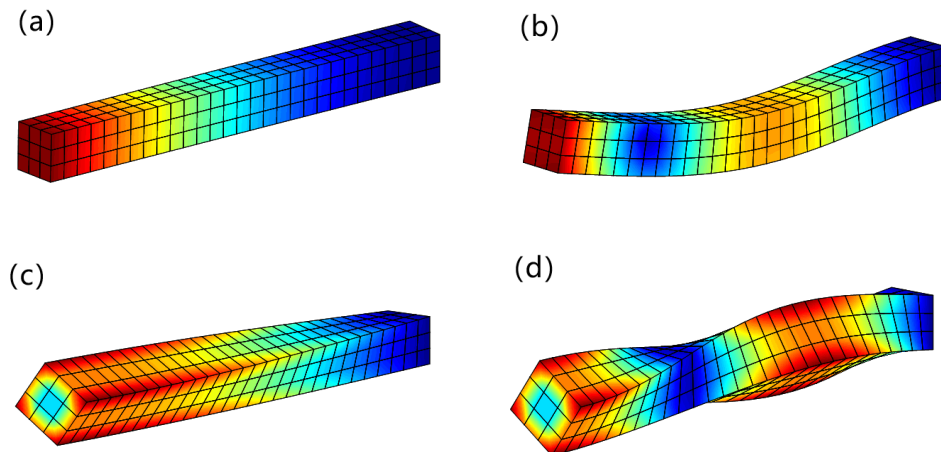Fig. 9. First flexural (a), second flexural (b), first torsional (c) and second torsional (d) modes for a CF square beam ($L = b \times 10$), L9.

5.2. Thin-walled beam structures

Free vibration analyses of a thin-walled C-shaped beam were carried out next for the assessment of the present beam model. The geometry of the cross-section is shown in Fig. 10(a). The sides of the cross-section are a =0.2 m and $b = a$. The thicknesses are $t = a/10$, and the length-to-side ratio $L/a = 10$. The material data are: Young modulus, E =198 GPa; Poisson ratio, ν =0.3; Material density ρ =7850 kg/m^3. Various order LE models are considered in the following analysis and some cross-sectional discretizations are shown in Figs. 10(b)–(f) for illustrative purposes.
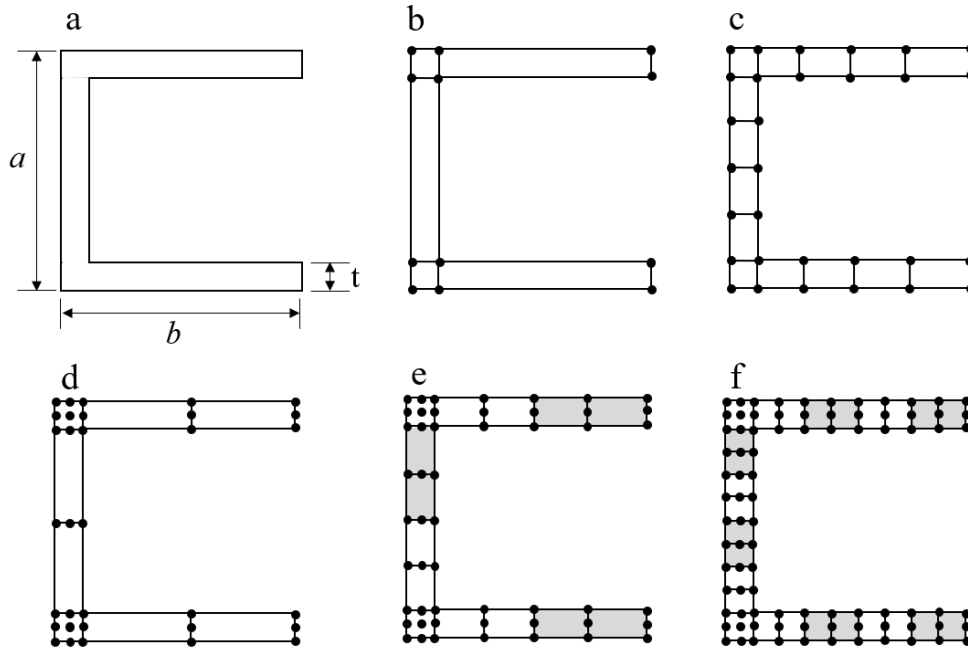

Fig. 10. C-shaped cross-section and LE discretizations. (a) C-shaped cross-section. (b) 5L4. (c) 14L4. (d) 5L9. (e) 8L9. (f) 14L9.

Table 3 shows the first eight natural frequencies (Hz) of the SS C-shaped cross-section beam. The results from the present LE models are compared to those from CUF(LE)-Navier theory and reference FE results from Ref. [52]. Various LE models are considered in the table as shown in Fig. 10. L4 models from 5 to 14 elements, and L9 models from 5 to 14 elements prove the accuracy of the proposed solution by comparing with the CUF(LE)-Navier solution. The results show that L9 models are affected by errors that are lower then 3% with respect to the 3D FEM solutions. On the other hand, considerable errors are produced by lower-order beam models in the higher frequencies range. The reason lower order L4 models do not give good results is that models from 5L4 to 14L4 do not have enough DOFs to characterize the shell-like modes. This aspect is clarified from Fig. 11, which shows the modes of vibrations by the 5L9 model.

Fig. 11 shows the first nine modes of the beam with SS boundary conditions obtained from the CUF-DSM analysis when using a 5L9 LE model. The first three modes (see Figs. 11(a)–(c)) are flexural mode, while all the later modes (Figs. 11(d)–(i)) show the coupled modes. The ability of 1D DSM-LE models in dealing with 2D shell-like analyses is documented in the present works. It is worth noting that arbitrarily complex modes

Table 3. First eight natural frequencies (Hz) related of the SS C-shaped cross-section beam

Model	Natural frequencies							
	1	2	3	4	5	6	7	8
FEM [52]								
3D FEM coarse	69.019	122.172	213.841	266.065	295.383	333.546	376.303	397.905
3D FEM finer	68.894	122.152	213.405	266.418	293.450	331.633	374.324	395.995
CUF (LE)-Navier [52]								
5 × L4	71.399	125.190	230.710	269.411	966.524	978.398	461.403	1011.057
14 × L4	69.700	122.510	220.824	267.473	457.367	490.185	417.933	530.673
5 × L9	69.360	122.256	218.971	267.083	314.103	350.559	409.009	414.623
8 × L9	69.158	122.173	215.103	266.894	300.941	339.205	383.042	404.349
14 × L9	68.995	122.149	214.018	266.780	297.059	335.286	377.374	400.022
Current theory								
5 × L4	71.399	125.190	230.710	269.411	966.524	978.398	461.403	1011.057
14 × L4	69.700	122.510	220.824	267.473	457.367	490.185	417.933	530.673
5 × L9	69.360	122.256	218.971	267.083	314.103	350.559	409.009	414.623
8 × L9	69.158	122.173	215.103	266.894	300.941	339.205	383.042	404.349
14 × L9	68.995	122.149	214.018	266.780	297.058	335.286	377.374	400.022
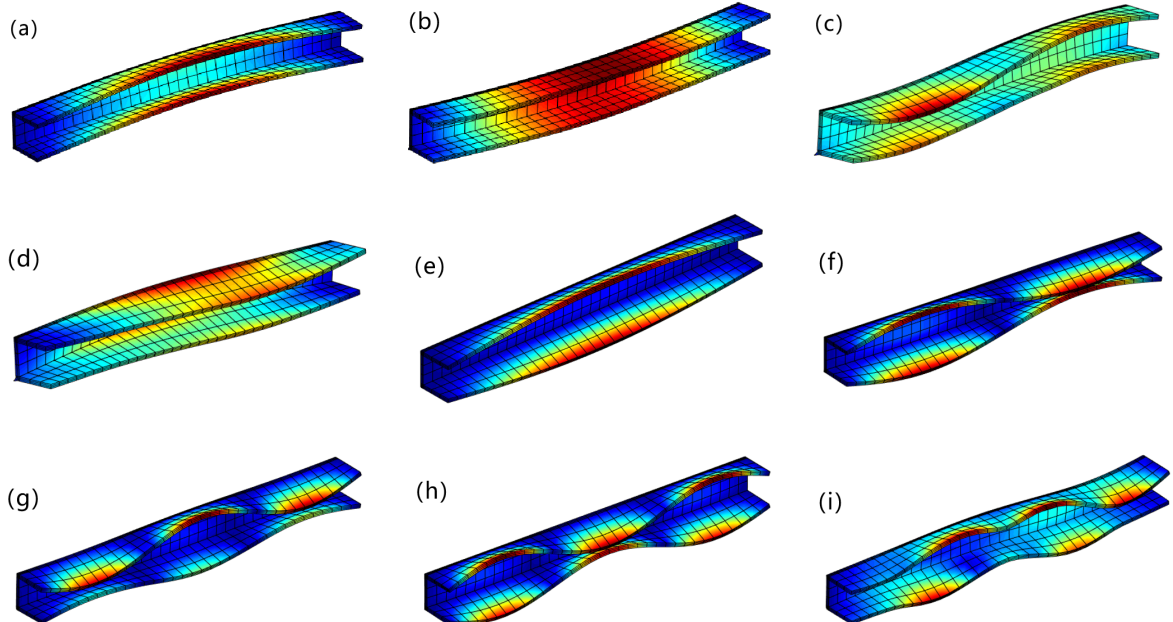
Fig. 11. Uncoupled (a-c) and coupled (d-f) modal shapes for a SS C-shaped cross-section beam ($L = a \times 10$), 5L9.

can be obtained by using only one element in the length direction by using the DSM, because the DSM provides the exact solution of the differential equations of the motion once the structural model has been formulated. In addition, each variable has a precise physical meaning by using Lagrange-type polynomials.

Table 4. First eight natural frequencies (Hz) related of the CF C-shaped cross-section beam for $L/a = 10$

Model	DOFs	Natural frequencies						
		1	2	3	4	5	6	7
FEM								
3D FEM coarse	62854	32.233	44.223	105.569	139.126	257.324	286.801	299.924
3D FEM finer	125706	32.089	44.208	105.429	138.793	257.131	283.633	297.873
Current theory								
5 × L4	60	33.253	45.264	107.148	145.662	266.540	339.104	501.316
14 × L4	150	32.600	44.324	106.060	141.450	259.421	318.894	450.373
5 × L9	165	32.443	44.246	105.816	140.640	258.211	304.028	314.907
8 × L9	255	32.278	44.220	105.599	139.543	257.497	290.528	302.835
14 × L9	435	32.182	44.211	105.503	139.117	257.253	286.672	299.916

In order to prove that DSM-LE can also provide accurate solutions for thin-walled beam structures with different boundary conditions, Table 4 shows first eight natural frequencies (Hz) related of the CF C-shaped cross-section beam for $L/a = 10$. Various LE models are considered in the table as shown in Fig. 10. FEM results from various ABAQUS models are also shown in Table 4. The ABQ C3D20 model with 125706 DOFs (finer) and 62854 DOFs (coarse) is adopted. From rows 3 to 7, the 14L9 model always shows the best accuracy among five different LE models because it has enough DOFs. In the first five natural frequencies, the percentage differences between the L4 models and the ABQ C3D20 model are small. Starting from the 6th frequency, the L4 model cannot produce reasonable results anymore. Especially for the 8th frequency, the percentage difference of the 5L4 and 14L4 model from the ABQ C3D20 model are 84.81% and 48.41%, respectively. The reason the L4 model cannot give good results is that L4 models do not have enough DOFs to characterize the shell-like modes. This aspect is also clarified from Fig. 12, which shows the modes of vibrations by the 5L9 model.

Fig. 12 shows the first eight modes of the beam with CF boundary conditions obtained from the CUF-DSM analysis when using a 5L9 LE model. The first five modes (see Figs. 12(a)–(e)) are uncoupled mode, while all the later modes (Figs. 12(f)–(h)) show the coupled modes. The ability of 1D DSM-LE models in dealing with 2D shell-like analyses for thin-walled beam structures with different boundary conditions is documented in the present works.

In order to further reflect the computational efficiency of this method, Table 5 shows first seven natural frequencies (Hz) related of the CF C-shaped cross-section beam for $L/a = 5$. Various LE models are considered in the table as shown in Fig. 10. FEM results from ABQ C3D20 models with 62854 DOFs (finer) and 31292 DOFs (coarse) are also shown in Table 5. The results illustrate that the DSM-LE can achieve comparable accuracy to a FEM model while requiring a significantly shorter calculation time, typically
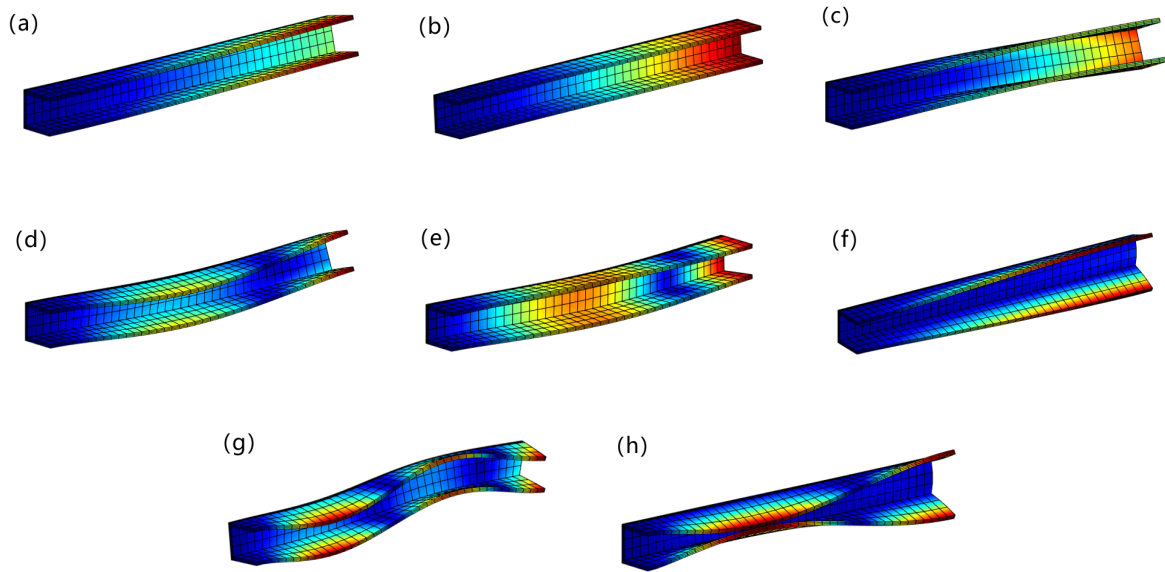
Fig. 12. Uncoupled (a-e) and coupled (f-h) modal shapes for a CF C-shaped cross-section beam ($L = a \times 10$), 5L9.

around 1 to 2 times faster. This is even more remarkable considering that the FEM model uses an optimised commercial solver while the DSM-LE runs as a research code in Matlab. This is due to the J_0 count solution technique presented in this paper, which greatly improves the computational efficiency, and the merit of the DSM is brought into full play.

Table 5. First seven natural frequencies (Hz) related of the CF C-shaped cross-section beam for $L/a = 5$

Model	DOFs	Natural frequencies							Time(s)
		1	2	3	4	5	6	7	
FEM									
3D FEM coarse	31292	93.452	170.981	298.535	348.665	381.341	414.005	617.638	36.00
3D FEM finer	62584	93.194	170.592	295.751	347.635	379.253	410.764	612.586	59.00
Current theory									
$5 \times$ L4	60	97.643	175.803	356.999	452.262	898.287	930.900	967.509	0.95
$14 \times$ L4	150	94.928	171.495	351.733	416.394	457.858	542.390	722.540	5.11
$5 \times$ L9	165	94.353	171.060	315.900	350.837	409.526	429.649	634.275	5.93
$8 \times$ L9	255	93.640	170.738	302.783	348.861	386.618	419.013	624.405	13.89
$14 \times$ L9	435	93.361	170.633	298.875	348.138	381.639	414.531	618.391	29.38

5.3. Stiffened panel structures

Free vibration analyses of a stiffened panel were carried out next for the assessment of the present approach. A stiffened panel consisting of the stringer component and panel component is a common research object which is shown as Fig. 13. In the CW approach,

each component is modeled individually and simultaneously by using CUF beam elements and the geometry of the cross-section is shown in Fig. 14(a). The sides of the cross-section are a_1 =0.096m, a_2 =0.032m, b_1 =0.1m and b_2 =0.2m. The length of total panel is 1.5m. The relevant material properties are shown in Table 6. Various order LE models are considered in the following analysis and some cross-sectional discretizations are shown in Figs. 14(b)–(f) for illustrative purposes.
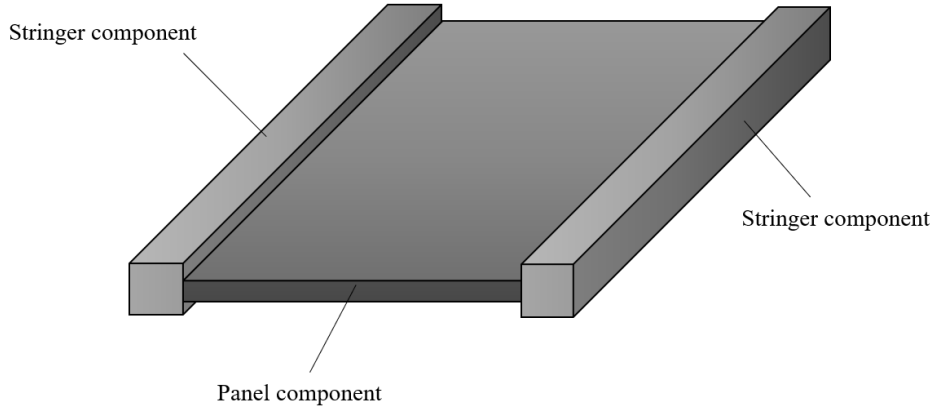

Fig. 13.   Component-wise approach for a stiffened panel structure.

Table 6. Material properties of stiffened panel structure.

Material	Elastic modulus (GPa)	Poisson ratio	Mass density (kg/m^3)
Stringer	210	0.2	7850
Panel	69	0.3	2500

Table 7 shows the first six natural frequencies (Hz) of the stiffened panel for different boundary conditions (BCs), namely, simply supported (SS) and clamped–free (CF) BCs. The solutions for various LE models considering in Fig. 14 are obtained using the CUF(LE)-DSM. The results are compared to FEM solutions from ABAQUS models which are referred to as ABQ C3D20 model with 91423 DOFs (coarse) and 182845 DOFs (finer). In the analysis, the 10L9 model always shows the best accuracy among five different LE models because it has enough DOFs. In the first one, three, four and six natural frequencies (flexural modes), the percentage differences between the L4 models and the ABQ C3D20 model are small. In the first two and five natural frequencies (shell-like modes), the L4 model and 7L9 model cannot produce reasonable results anymore. The reason the is that L4 models and 7L9 model do not have enough DOFs to characterize the shell-like modes under different boundary conditions.

In addition, the first six modal shapes for a SS stiffened panel structure attained from 8L9 models are depicted in Fig. 15. The first one, three, four and six modes are flexural modes, respectively. The two and five modes are shell-like modes. It has been demonstrated from Table 7 and Fig. 15 that 1D higher-order models based on LE model are necessary to detect shell-like modes of combined structures such as reinforced panel.
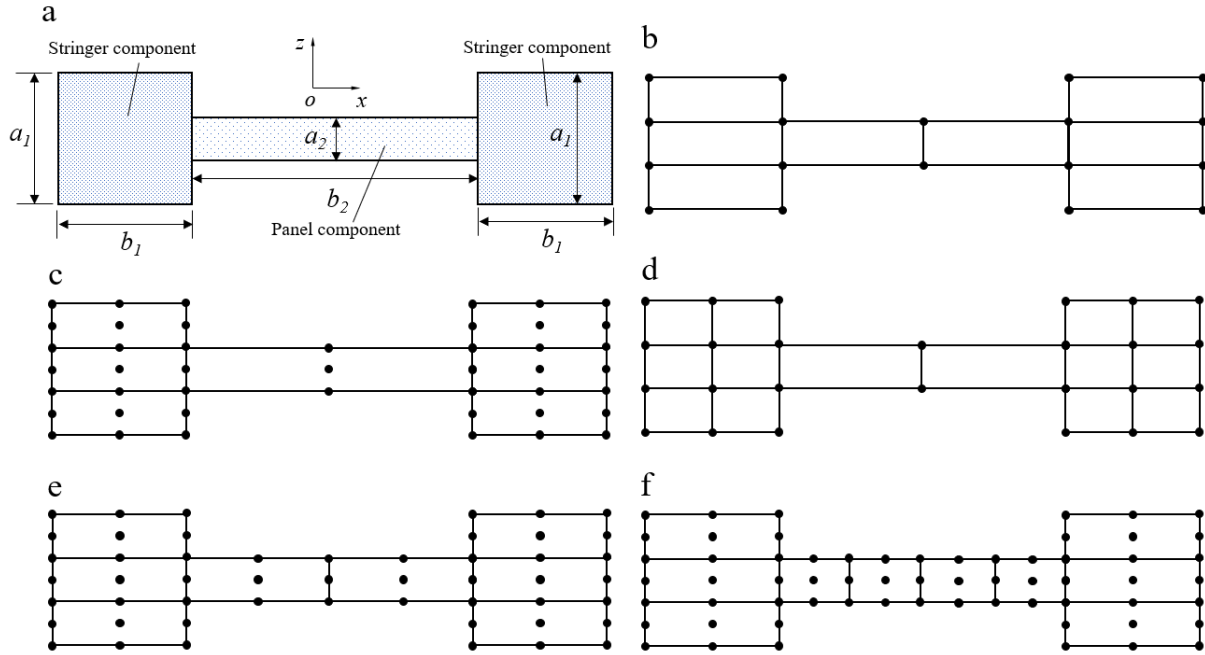
Fig. 14. Stiffened panel cross-section and LE discretizations. (a) Stiffened panel cross-section. (b) 8L4. (c) 7L9. (d) 14L4. (e) 8L9. (f) 10L9.

Table 7. First six natural frequencies (Hz) of the stiffened panel for different boundary conditions.

| BCs	Model	DOFs	Natural frequencies					
			1	2	3	4	5	6
SS	3D FEM coarse	91423	95.218	252.87	364.44	373.96	526.55	816.93
	3D FEM finer	182845	95.215	251.11	364.28	373.94	522.48	816.82
	$8 \times$ L4	162	96.221	295.78	367.01	378.59	628.06	829.47
	$14 \times$ L4	234	95.826	294.38	365.85	377.06	624.05	826.17
	$7 \times$ L9	405	95.166	293.92	365.57	374.96	622.92	817.84
	$8 \times$ L9	459	95.224	262.72	364.73	374.05	537.36	817.50
	$10 \times$ L9	567	95.218	258.46	364.65	373.97	530.21	817.01
CF	3D FEM coarse	91423	34.093	143.35	153.59	209.97	383.46	572.08
	3D FEM finer	182845	34.074	142.77	153.52	209.91	379.70	571.85
	$8 \times$ L4	162	34.427	154.41	160.01	212.31	472.05	580.06
	$14 \times$ L4	234	34.297	154.06	159.41	211.52	468.74	577.90
	$7 \times$ L9	405	34.080	154.05	159.27	209.88	468.21	572.36
	$8 \times$ L9	459	34.078	148.95	153.68	209.91	395.17	572.25
	$10 \times$ L9	567	34.075	147.87	153.61	209.94	388.85	572.06
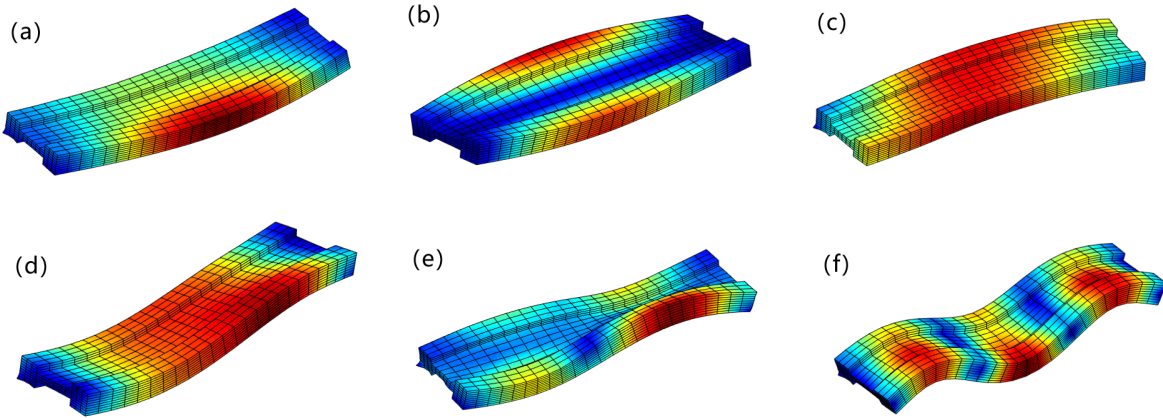
Fig. 15. Flexural (a,c,d,f) and shell-like (b,e) modal shapes for a SS stiffened panel structure ($L = a_1 \times 15$), 8L9.

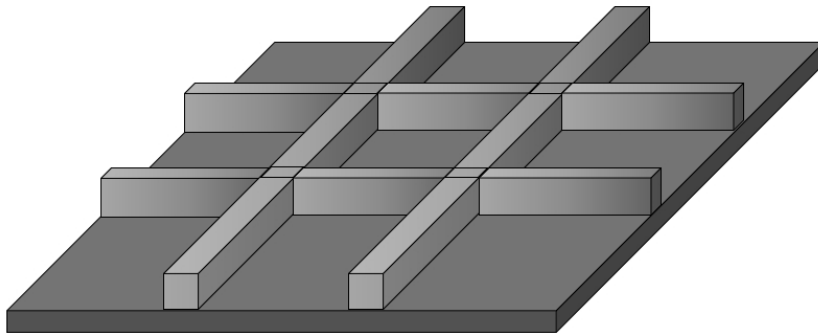## 5.4. Reinforced panels with four stifeners

Fig. 16. Reinforced panels with four stifeners.

This section extends the use of the present approach to a reinforced panel structures. For purpose of description, in this work the same notation as used in [66] has been adopted. Therefore, the symbolism C-F-F-F identifies a plate with the edges $y = 0, x = a, y = b$, and $x = 0$ having clamped, free, free, free boundary conditions, respectively (see Fig. 1). Similarly S-F-S-F denotes a plate with two opposite simply-supported edges and two opposite free edges. The dynamic analysis of a reinforced panel with four stiffeners as shwon in Fig. 16 is presented and the geometry of the structure is shown in Fig. 17. The sides of the cross-section are a =0.5m, b =0.5m, $h_1 = h_2$ =0.2m and t =0.2m. The material data are: Young modulus, E =198 GPa; Poisson ratio, ν =0.3; Material density ρ =7850 kg/m^3. Various order LE models are considered in the following analysis and some cross-sectional discretizations are shown in Figs. 18(a)–(c) for illustrative purposes.

Table 8 shows the first seven natural frequencies (Hz) of the reinforced panel with four stiffeners for different boundary conditions (BCs), namely, S-F-S-F and C-F-F-F BCs. The solutions for various LE models considering in Fig. 18 are obtained using the
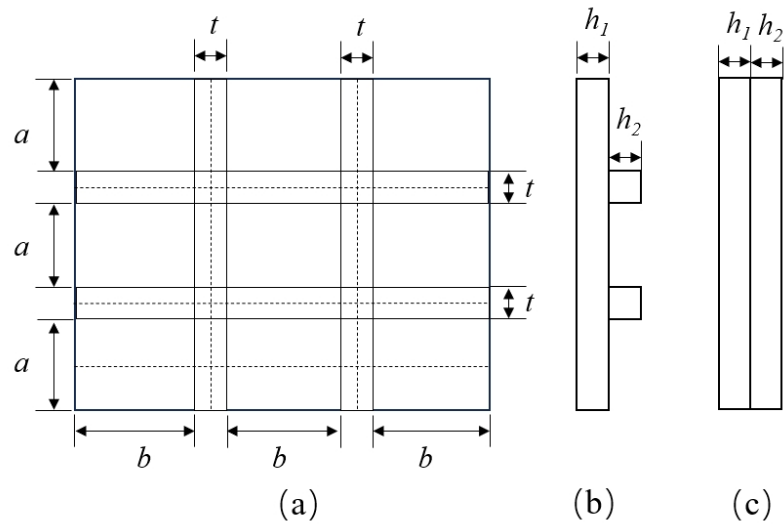
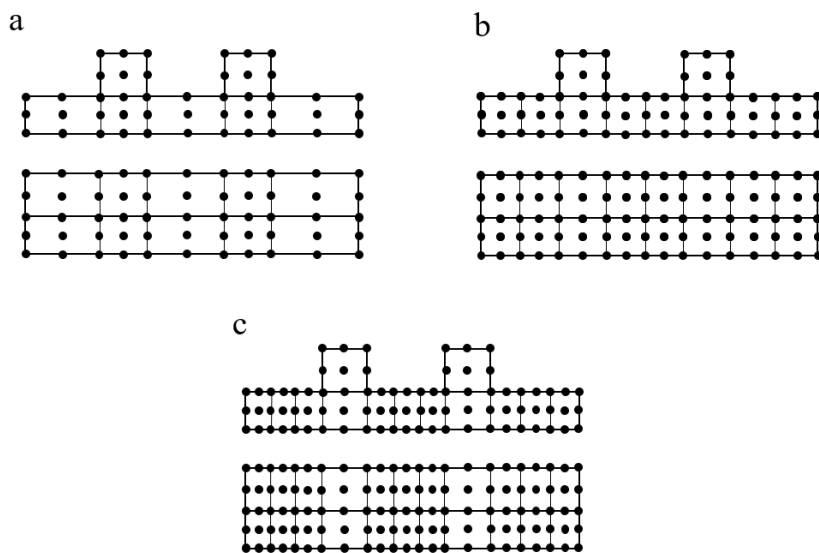Fig. 17. The geometry of the reinforced panels with four stifeners.

Fig. 18. Reinforced panels cross-section and LE discretizations. (a) 7L9 & 10L9. (b) 10L9 & 16L9. (c) 13L9 & 22L9.

Table 8. The first seven natural frequencies (Hz) of the reinforced panel with four stiffeners for different boundary conditions (BCs), namely, simply supported (SS) and clamped–free (CF) BCs.

BCs	Model	DOFs	Natural frequencies						
			1	2	3	4	5	6	7
SS	3D FEM coarse	10996	177.86	231.98	541.18	578.89	585.71	603.43	754.92
	3D FEM finer	38845	176.97	228.83	539.40	573.71	580.14	593.68	751.05
	$7 \times$ L9 & $10 \times$ L9	555	178.75	233.37	542.03	583.69	587.88	606.15	755.76
	$10 \times$ L9 & $16 \times$ L9	825	178.02	231.62	540.92	578.16	585.13	602.27	753.23
	$13 \times$ L9 & $22 \times$ L9	1095	177.35	231.02	540.13	576.79	584.03	600.54	752.49
CF	3D FEM coarse	10996	70.655	135.89	252.97	357.35	443.92	459.93	630.37
	3D FEM finer	38845	70.031	132.74	252.01	354.09	434.92	455.05	629.83
	$7 \times$ L9 & $10 \times$ L9	555	70.705	135.66	253.24	357.93	444.61	463.92	631.89
	$10 \times$ L9 & $16 \times$ L9	825	70.505	134.41	252.56	356.45	440.85	458.94	631.05
	$13 \times$ L9 & $22 \times$ L9	1095	70.309	134.03	252.39	355.88	439.78	457.98	630.51

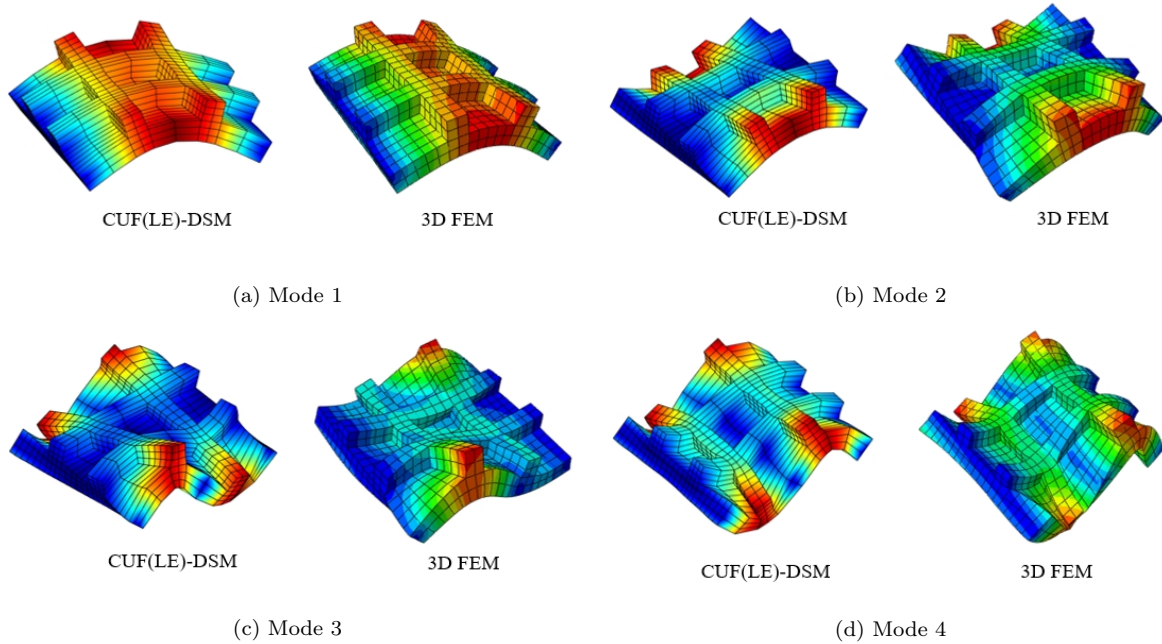
(a) Mode 1

(b) Mode 2

(c) Mode 3

(d) Mode 4

Fig. 19. The first four mode shapes for a SS reinforced panels with four stifeners evaluated with FEM models.

CUF(LE)-DSM. The results are compared to FEM solutions from ABAQUS models which are referred to as ABQ C3D20 model with 10996 DOFs (coarse) and 38845 DOFs (finer). The comparison between the the results by FEM and those from the present models demonstrate the efficiency of the CUF(LE)-DSM models, in fact, a higher accuracy is reached with a reduction in the computational costs. In the analysis, the 13 × L9 & 22 × L9 model always shows the best accuracy among five different LE models because it has enough DOFs.

Fig.19 shows the first four mode shapes for a S-F-S-F reinforced panels with four stifeners evaluated with FEM models. 3D FEM model is used as a reference solution which is made using only 3D elements for all the components of the plate and stringers. The results from the present approach are comparable with those from the 3D FEM model in terms of accuracy, but can be achieved using 13% of the degrees of freedom.

6. Conclusions

This paper has developed new CUF-DS models for the efficient analysis of the free vibrations of solid beams, thin-walled structures and reinforced panels with arbitrary boundary conditions. By exploiting the Carrera unified formulation (CUF) and Lagrange polynomials to discretize the beam cross-sectional kinematics, refined models with only displacement variables have been developed. The resulting DS matrix is applied using the extended Wittrick–Williams algorithm to compute the natural frequencies and mode shapes of some solid and thin-walled structures. Using those approaches, higher order models that are able to deal with shear deformation and higher-order effects, such as warping, can be captured straightforwardly with the help of CUF. The following considerations arise from the comparison of the present approach with results available in the literature and 3D FEM solutions from commercial software:

- A higher-order exact DS formulations have been developed by first using Lagrange polynomials to define the displacement field above the cross-section of the beam. The Lagrange-based formulation offers enhanced capabilities compared to Talyor-based CUF modelling. The accuracy improves with a higher order of Lagrange polynomials.

- The mode appearance can be interchanged in lower-order LE models (L4), even if a large number of elements on the cross-section are used. By using higher Lagrange polynomials (L9 or L16) with fewer elements, interchange can also be shown.

- The resulting LE-DSM based on Component-Wise (CW) can be used for the whole cross-section or can be introduced by dividing the cross-section into various sub-domains, because Lagrange elements can be used to model the displacement variables in each structural component at the cross-sectional level. This characteristic allows us to separately model.

- Analytical expressions of the J_0 count have been developed for the Wittrick–Williams (WW) algorithm. With the J_0 problem resolved, there is no need to split a large dynamic stiffness element into smaller ones unnecessarily as the majority of existing

works did. Therefore, very few DOFs are required for beam structures, which has made the DSM to be highly efficient.

The results agree with those obtained using ABAQUS FEM models and with those from the literature. The present analytical CUF(LE)-DSM formulation clearly demonstrates its efficiency over 3D FEM solutions and the capabilities of capturing higher-order refined effects. The investigation provides optimism for future studies on the dynamic analysis of composite structures.

References

[1] L. Euler. De curvis elasticis. *Lausanne and Geneva: Bousquet*, 1744.
[2] S.P. Timoshenko. On the transverse vibrations of bars of uniform cross section. *Philosophical Magazine*, 43(1):125–131, 1992.
[3] S.P. Timoshenko. On the correction for shear of the differential equation for transverse vibrations of prismatic bars. *Philosophical Magazine*, 41(245):744–746, 1921.
[4] V.V. Novozhilov. *Theory of Elasticity*. Pergamon, Elmsford, 1961.
[5] K. Kapania and S. Raciti. Recent advances in analysis of laminated beams and plates. Part I - Sheareffects and buckling. *AIAA Journal*, 27(7):923–935, 1989.
[6] K. Kapania and S. Raciti. Recent Advances in Analysis of Laminated Beams and Plates, Part II: Vibrations and Wave Propagation. *AIAA Journal*, 27(7):935–946, 1989.
[7] E. Carrera, A. Pagani, M. Petrolo, and E. Zappino. Recent developments on refined theories for beams with applications. *Mechanical Engineering Reviews*, 2(2), 2015.
[8] S.P.Timoshenko and J.N.Goodier. *Theory of Elasticity*. McGraw-Hill, 1970.
[9] R. Gonçalves, D. Camotim, and Pedro Dinis. *Generalised Beam Theory to Analyse the Buckling Behaviour of Aluminium or Stainless Steel Open and Closed Thin-Walled Members*, pages 843–852. 2018.
[10] A. Garg, H. D. Chalak, A. M. Zenkour, M. O. Belarbi, and R. Sahoo. Bending and free vibration analysis of symmetric and unsymmetric functionally graded CNT reinforced sandwich beams containing softcore. *Thin-Walled Structures*, 170:108626, 2022.
[11] J. Náprstek and C. Fischer. Static and dynamic analysis of beam assemblies using a differential system on an oriented graph. *Computers and Structures*, 155:28–41, 2015.
[12] A. Alibakhshi, S. Dastjerdi, N. Fantuzzi, and S. Rahmanian. Nonlinear free and forced vibrations of a fiber-reinforced dielectric elastomer-based microbeam. *International Journal of Non-Linear Mechanics*, 144:104092, 2022.
[13] I.S.Sokolnikoff. *Mathematical Theory of Elasticity*. McGraw-Hil, 1956.
[14] N.G.Stephen. Timoshenko's shear coefficient from a beam subjected to gravity loading. *Journal of Applied Mechanics*, 47:121–127, 1980.
[15] J.R.Hutchinson. Shear coefficients for timoshenko beam theory. *Journal of Applied Mechanics*, 68(1):87–92, 2001.
[16] J.J.Jensen. On the shear coefficient in Timoshenko's beam theory. *Journal of Sound and Vibration*, 87(4):621–635, 1983.
[17] T. Kaneko. On Timoshenko's correction for shear in vibrating beams. *Journal of Physics D: Applied Physics*, 8:1927–1936, 1975.
[18] S. B. Dong, C. Alpdogan, and E. Taciroglu. Much ado about shear correction factors in Timoshenko beam theory. *International Journal of Solids and Structures*, 47:1651–1665, 2010.
[19] R.El Fatmiand H. Zenzri. On the structural behavior and the Saint Venant solution in the exact beam theory: Application to laminated composite beams. *Computers and Structures*, 80:1441–1456, 2002.
[20] R. El Fatmi. Non-uniform warping including the effects of torsion and shear forces. Part II: Analytical and numerical applications. *International Journal of Solids and Structures*, 44:5930–5952, 2007.
[21] R. El Fatmi. Non-uniform warping including the effects of torsion and shear forces. Part I: A general beam theory. *International Journal of Solids and Structures*, 44:5912–5929, 2007.

[22] P. Ladevèze and J. Simmonds. New concepts for linear beam theory with arbitrary geometry and loading. *European Journal of Mechanics, A/Solids*, 17:377–402, 1998.

[23] P. Ladevèze, P. Sanchez, and J.G. Simmonds. Beamlike (Saint-Venant) solutions for fully anisotropic elastic tubes of arbitrary closed cross section. *International Journal of Solids and Structures*, 41:1925–1944, 2004.

[24] O. Rand. Free vibration of thin-walled composite blades. *Composite Structures*, 28(2):169–180, 1994.

[25] C. Kim and S.R. White. Thick-walled composite beam theory including 3-D elastic effects and torsional warping. *International Journal of Solids and Structures*, 34:4237–4259, 1997.

[26] V.L. Berdichevsky and E. Armanios amd A. Badir. Theory of anisotropic thin-walled closed-cross-section beams. *Composites Engineering*, 2:411–432, 1992.

[27] V.V. Volovoi, D.H. Hodges, V.L. Berdichevsky, and V.G. Sutyrin. Asymptotic theory for static behavior of elastic anisotropic I-beams. *International Journal of Solids and Structures*, 36:1017–1043, 1999.

[28] B. Popescu and D.H. Hodges. On asymptotically correct Timoshenko-like anisotropic beam theory. *International Journal of Solids and Structures*, 37:535–558, 2000.

[29] W. Yu, V.V. Volovoi, D.H. Hodges, and X. Hong. Validation of the variational asymptotic beam sectional analysis (VABS). *AIAA Journal*, 40:2105–2113, 2002.

[30] W. Yu and D.H. Hodges. Elasticity solutions versus asymptotic sectional analysis of homogeneous, isotropic, prismatic beams. *Journal of Applied Mechanics*, 71:15–23, 2004.

[31] W. Yu and D.H. Hodges. Generalized Timoshenko theory of the variational asymptotic beam sectional analysis. *Journal of the American Helicopter Society*, 50:46–55, 2005.

[32] J.S. Kim and K.W. Wang. Vibration analysis of composite beams with end effects via the formal asymptotic method. *Journal of Vibration and Acoustics*, 132:041003, 2010.

[33] R.D. Firouz-Abad, H. Haddadpour, and A.B. Novinzadehb. An asymptotic solution to transverse free vibrations of variable-section beams. *Journal of Sound and Vibration*, 304:530–540, 2007.

[34] R.D. Firouz-Abad, H. Haddadpour, and A.B. Novinzadehb. Eine erweiterung der technischen biegetheorie zur berechnung prismatischer faltwerke (Extension of the engineer's theory of bending to the analysis of folded plate structures). *Der Stahlbau*, 35:161–171, 1996.

[35] R. Schardt. Generalized beam theory an adequate method for coupled stability problems. *Thin-Walled Structures*, 19:161–180, 1994.

[36] N. Silvestre and D. Camotim. First-order generalised beam theory for arbitrary orthotropic materials. *Thin-Walled Structures*, 40:755–789, 2002.

[37] N. Silvestre. Second-order generalised beam theory for arbitrary orthotropic materials. *Thin-Walled Structures*, 40:791–820, 2002.

[38] N. Silvestre. Generalised beam theory to analyse the buckling behaviour of circular cylindrical shells and tubes. *Thin-Walled Structures*, 45:185–198, 2007.

[39] R. Bebiano, N. Silvestre, and D. Camotim. Local and global vibration of thin-walled members subjected to compression and non-uniform bending. *Journal of Sound and Vibration*, 345:509–535, 2008.

[40] K. Washizu. *Variational Methods in Elasticity and Plasticity.* Pergamon, Oxford, 1968.

[41] E. Carrera, G. Giunta, and M. Petrolo. *Beam Structures Beam Structures.* 2001.

[42] E. Carrera. A class of two dimensional theories for multilayered plates analysis. *Atti Accademia delle Scienze di Torino, Memorie Scienze Fisiche*, 19–20:49–87, 1995.

[43] E. Carrera. Theories and finite elements for multilayered, anisotropic, composite plates and shells. *Archives of Computational Methods in Engineering*, 9:87–140, 2002.

[44] E. Carrera. Theories and finite elements for multilayered and shells: a unified compact formulation with numerical assessment and benchmarking. *Archives of Computational Methods in Engineering*, 10:216–296, 2003.

[45] E. Carrera and S. Brischetto. Analysis of thickness locking in classical, refined and mixed multilayered plate theories. *Composite Structures*, 82:549–562, 2008.

[46] E. Carrera, M. Cinefra, E. Zappino, and M. Petrolo. *Finite Element Analysis of Structures through Unified Formulation.* John Wiley & Sons, 2014.

[47] E. Carrera and M. Petrolo. Refined beam elements with only displacement variables and plate/shell capabilities. *Meccanica*, 47(3):537–556, 2012.

[48] E. Carrera and M. Petrolo. Refined one-dimensional formulations for laminated structure analysis. *AIAA Journal*, 50(1):176–189, 2012.

[49] G. Giunta, D. Crisafulli, S. Belouettar, and E. Carrera. Hierarchical theories for the free vibration analysis of functionally graded beams. *Composite Structures*, 94(1):68–74, 2011.

[50] G. Giunta, F. Biscani, S. Belouettar, A. J.M. Ferreira, and E. Carrera. Free vibration analysis of composite beams via refined theories. *Composites Part B: Engineering*, 44(1):540–552, 2013.

[51] G. Giunta, S. Belouettar, H. Nasser, EH. Kiefer-Kamal, and T. Thielen. Hierarchical models for the static analysis of three-dimensional sandwich beam structures. *Composite Structures*, 133:1284–1301, 2015.

[52] M. Dan, A. Pagani, and E. Carrera. Free vibration analysis of simply supported beams with solid and thin-walled cross-sections using higher-order theories based on displacement variables. *Thin-Walled Structures*, 98:478–495, 2016.

[53] J. R. Banerjee. Free vibration of centrifugally stiffened uniform and tapered beams using the dynamic stiffness method. *Journal of Sound and Vibration*, 233(5):857–875, jun 2000.

[54] J. R. Banerjee and A. Ananthapuvirajah. Coupled axial-bending dynamic stiffness matrix for beam elements. *Computers and Structures*, 215:1–9, 2019.

[55] J. R. Banerjee. Review of the dynamic stiffness method for free-vibration analysis of beams. *Transportation Safety and Environment*, 1(2):106–116, 2019.

[56] J. R. Banerjee and A. Ananthapuvirajah. An exact dynamic stiffness matrix for a beam incorporating Rayleigh–Love and Timoshenko theories. *International Journal of Mechanical Sciences*, 150(June 2018):337–347, 2019.

[57] J. R. Banerjee and F. W. Williams. Further flexural vibration curves for axially loaded beams with linear or parabolic taper. *Journal of sound and vibration*, 102(3):315–327, oct 1985.

[58] J. R. Banerjee. Dynamic stiffness formulation and its application for a combined beam and a two degree-of-freedom system. *Journal of Vibration and Acoustics, Transactions of the ASME*, 125(3):351–358, 2003.

[59] J. R. Banerjee. Dynamic stiffness formulation for structural elements: A general approach. *Computers and Structures*, 63(1):101–103, 1997.

[60] J. R. Banerjee and F. W. Williams. Exact Bernoulli–Euler dynamic stiffness matrix for a range of tapered beams. *International Journal for Numerical Methods in Engineering*, 21(12):2289–2302, 1985.

[61] X. Liu, C. Xie, and C. Dan. Exact Free Vibration Analysis for Plate Built-Up Structures under Comprehensive Combinations of Boundary Conditions. *Shock and Vibration*, 2020.

[62] X. Liu and J.R. Banerjee. An exact spectral-dynamic stiffness method for free flexural vibration analysis of orthotropic composite plate assemblies - Part I: Theory. *Composite Structures*, 132:1274–1287, 2015.

[63] X. Liu and J.R. Banerjee. An exact spectral-dynamic stiffness method for free flexural vibration analysis of orthotropic composite plate assemblies - Part II: Applications. *Composite Structures*, 132:1288–1302, 2015.

[64] X. Liu, X. Liu, S. Adhikari, and X. Zhao. An analytical framework for broadband dynamic analysis of plate built-up structures with uncertain viscoelastic boundary or connection conditions. *Mechanical Systems and Signal Processing*, 177(November 2021):109121, 2022.

[65] X. Liu, X. Liu, S. Adhikari, and S. Yin. Extended Wittrick–Williams algorithm for eigenvalue solution of stochastic dynamic stiffness method. *Mechanical Systems and Signal Processing*, 166(September 2021):108354, 2022.

[66] A. Pagani, E. Carrera, J. R. Banerjee, P. H. Cabral, G. Caprio, and A. Prado. Free vibration analysis of composite plates by higher-order 1D dynamic stiffness elements and experiments. *Composite Structures*, 118:654–663, 2014.

[67] A. Pagani, M. Boscolo, J. R. Banerjee, and E. Carrera. Exact dynamic stiffness elements based on one-dimensional higher-order theories for free vibration analysis of solid and thin-walled structures. *Journal of Sound and Vibration*, 332(23):6104–6127, 2013.

[68] A. Pagani, E. Carrera, M. Boscolo, and J. R. Banerjee. Refined dynamic stiffness elements applied to free vibration analysis of generally laminated composite beams with arbitrary boundary conditions. *Composite Structures*, 110(1):305–316, 2014.

[69] J.N. Reddy. *Mechanics of Laminated Composite Plates and Shells: Theory and Analysis.* 2nd ed., CRC Press, 2004.

[70] S.W. Tsai. *Composites Design.* 4th ed. Dayton, Think Composites, 1988.

Acknowledgements